Journal of Iberian Geology (2023) 49:1–19
https://doi.org/10.1007/s41513-022-00202-6

RESEARCH PAPER

Geochemistry of Precambrian black shales from Ossa-Morena Zone (Portugal): depositional environment and possible source of metals

V. Laranjeira[1,2] · J. Ribeiro[3,4] · N. Moreira[5,6,7] · P. Nogueira[8,9] · D. Flores[1,2]

Received: 17 June 2022 / Accepted: 14 December 2022 / Published online: 9 January 2023

Abstract

The paleodepositional environments related to Ediacaran black shales from the *Série Negra* succession in Ossa-Morena tectonostratigraphic zone were investigated using their geochemical composition to identify the sedimentary sources and depositional conditions. Their potential for assisting the genesis of metal deposits was also discussed. The sedimentary sources of the black shales are related to the break up of a Cadomian magmatic-arc developed in the North Gondwana realm, where the Ossa-Morena Zone was located during late Ediacaran times, showing acidic to mixed signatures. Some ratios were calculated based on redox sensitive elements, indicating both anoxic and oxic paleoenvironmental conditions. The anoxic conditions were predominant and they were identified on samples with higher organic carbon content, emphasizing that the redox conditions favored organic matter preservation and the accumulation of selected metals. Considering the mode of occurrence, the elements Ag, Cd, Cu, Pb and Se are assumed to be preferentially associated with sulfides, whereas Mo and U are preferentially organically bound. The results reveal that the black shales from the *Série Negra* succession in Ossa-Morena Zone might represent a source of metals, which were probably remobilized during Variscan events.

Keywords Ediacaran · Black shales · Redox sensitive elements · Sedimentary sources · Source of metals

Geoquímica de las lutitas negras Precámbricas de la zona de Ossa-Morena (Portugal): ambiente deposicional y posible fuente de metales

Resumen

Los ambientes paleodeposicionales de las lutitas negras del Ediacárico de la sucesión *Série Negra* de la Zona de Ossa-Morena fueron investigados mediante análisis de su composición geoquímica, para identificar las fuentes sedimentarias y sus condiciones de deposición. También se discutió su potencial como fuente de metales, con implicaciones en la génesis de los yacimientos de esta zona tectonoestratigráfica. Las fuentes sedimentarias de las lutitas negras están relacionadas con la instalación y desmantelamiento del arco magmático Cadomiano desarrollado en el Norte de Gondwana durante el Ediacárico tardío, donde se localizaba la zona de Ossa-Morena, mostrando fuentes sedimentarias de origen magmática de naturaleza ácida a mixta. Basado en los elementos sensibles redox y sus proporciones, se identificó condiciones paleodeposicionales tanto anóxicas como óxicas. Las condiciones anóxicas son predominantes y se identificaron en muestras con mayor contenido de carbono orgánico, mostrando que las condiciones redox favorecieron la preservación de la materia orgánica y la acumulación de algunos metales. Considerando el modo de ocurrencia, se asume que los elementos Ag, Cd, Cu, Pb y Se están preferentemente asociados con sulfuros, mientras que Mo y U están preferentemente ligados con la materia orgánica. Los resultados indican que las lutitas negras de la sucesión *Série Negra* podrían representar una fuente de metales, probablemente removilizados y concentrados durante los eventos Variscos, participando en la génesis de los yacimientos metálicos de la Zona de Ossa-Morena.

Palabras clave Ediacárico · Lutitas negras · Elementos sensibles redox · Fuentes sedimentarias · Fuente de metales

✉ V. Laranjeira
vanessa.laranjeira@fc.up.pt

Extended author information available on the last page of the article

1 Introduction

Black shales are defined as fine-grained rocks with disperse organic matter (OM), where the total organic carbon (TOC) is above 0.5 wt% (Huyck, 1989; Trabucho-Alexandre, 2014); they are the result of the accumulation and preservation of the OM in the sediments mostly from reducing environments (Tourtelot, 1979; Wignall, 1994). Black shales are generally formed in marine anoxic bottom waters, although they can occur in a wide range of depositional environments (e.g. Ai et al., 2020; Gao et al., 2016; Potter et al., 1980; Schieber, 1978).

The use of geochemical proxies allows the characterization of paleodepositional environments at the time of sedimentation and diagenesis (e.g. Fang et al., 2019; Gao et al., 2016). The redox variations are mainly controlled by the availability of O_2 and H_2S, represented essentially by the presence of OM, sulfides and biological activity (e.g. El-Anwar et al., 2018; Ferreira et al., 2020; Jones & Manning, 1994) and can be evaluated based on the relationships between some trace elements, namely As, Cr, Co, Cu, Mo, Ni, U, V (Leventhal, 1993).

Black shales are significant in economic geology since they can be the source rock for hydrocarbons production and are often spatially associated with several types of ore deposits, mostly due to the enrichment of metals within black shales successions (e.g. Cortial et al., 1990; Gao et al., 2016; Kontinen & Hanski, 2015; Potter et al., 1980; Sáez et al., 2011; Sozinov, 1982; Suárez-Ruiz et al., 2012). Black shales, due to the active participation of the OM, provide the necessary redox conditions for an enrichment of metals in the sediments. Therefore, these rock units are a valuable source of metals for later mineralizing processes (Sozinov, 1982; Suárez-Ruiz et al., 2012 and references therein).

The occurrence of black shales is common and widespread in the geological record (Kunzmann et al., 2015; Sozinov, 1982; Tourtelot, 1979; Wang et al., 2019; Wignall, 1994). Several studies on Precambrian black shales have demonstrated their relevance on the recognition of paleogeographic conditions, depositional environments, processes affecting metamorphic complexes, as well as in ore deposits genesis (e.g. Fang et al., 2019; Kunzmann et al., 2015; Sozinov, 1982). The main sources of OM in Ediacaran rocks have been interpreted as result from the accumulation of prokaryotic (i.e. bacterial) and eukaryotic (i.e. algal) organisms (Ai et al., 2020).

Precambrian successions with black shales, specifically from the Ediacaran, occur in the southernmost tectonostratigraphic zone of Iberian Terrane, the Ossa-Morena Zone (OMZ), locally named the *Série Negra* succession (e.g. Carvalhosa, 1965; Gonçalves & Carvalhosa, 1994; Gonçalves & Oliveira, 1986; Oliveira et al., 1991). Previous investigations addressed its paleogeography, based on the petrographic and geochemical characterization of the inorganic fraction of the different lithologies of the Precambrian of OMZ, including the *Série Negra* succession (e.g. Chichorro et al., 2008; Lopes, 2015; Lopes et al., 2015; López-Guijarro, 2006; López-Guijarro et al., 2008; Oliveira et al., 2003; Pereira et al., 2006).

However, the black shales from the *Série Negra* were never investigated in detail. The first approach to the characterization of the OM present in the black shales from the *Série Negra* was recently presented in Laranjeira et al. (2023), where the petrographic observation allowed the identification of dispersed organic matter exhibiting graphitic features, disseminated as flakes in association with iron oxides.

Considering the importance of black shales for paleoenvironmental studies and its potential association with the genesis of ore deposits, this work is a contribution to the knowledge of the Ediacaran black shales from *Série Negra* of OMZ, discussing its geochemical features, establishing the depositional paleoenvironmental conditions and the sedimentary sources based on geochemical proxies. Moreover, the role of these black shales as a possible source of metals is discussed.

2 Geological setting

The Iberian Massif is characterized by the presence of stratigraphic units from Neoproterozoic to Upper Paleozoic, that are divided in several tectonostratigraphic zones, among which the OMZ (e.g. Dias et al., 2016; Ribeiro et al., 2007). The OMZ is a heterogeneous and complex tectonostratigraphic zone, with unique stratigraphic, magmatic and tectono-metamorphic features, due to the presence of two successive Wilson Cycles, namely the Cadomian and Variscan Cycles (e.g. Eguíluz et al., 2000; Moreira et al., 2014a; Oliveira et al., 1991; Quesada & Oliveira, 2019; Ribeiro et al., 2007, 2009).

The Ediacaran record exposed in the OMZ commonly includes the *Série Negra* succession, initially described both in Portugal by Carvalhosa (1965) and in Spain by Alia (1963) and Vegas (1968). This metasedimentary succession outcrops in the core of NW–SE Variscan regional structures, namely: (1) the northern edge of the OMZ, outlined by Tomar-Badajoz-Córdoba Shear Zone (Blastomylonitic Belt) and the Obejo-Valsequillo-Puebla de la Reina Domain; (2) the core of the Estremoz, Olivenza-Monesterio and Vila Boim Anticlines located in Central Domains of OMZ; and (3) in the Almadén de la Plata-Aracena, Montemor-o-Novo, Moura, Viana do Alentejo and Serpa regions, in the OMZ Southern Domains (e.g. Apalategui et al., 1990; Araújo

et al., 2013; Eguíluz et al., 2000; Moreira et al., 2014b; Oliveira et al., 1991; Pereira et al., 2006, 2012a; Quesada, 1990) (Fig. 1A). Two distinct metasedimentary units are included in the *Série Negra* Neoproterozic succession of the Blastomylonitic Belt, from the bottom to the top (e.g. Eguíluz et al., 2000; Oliveira et al., 1991, 2003; Pereira et al., 2006):

- Morenos Formation: siliceous shales, black metacherts and quartzites, meta-arkoses and metapsammites and garnet-bearing micaschists, sometimes with interlayered felsic and mafic meta-volcanic rocks (similar to Montemolín succession described in Spain).
- Mosteiros Formation: includes a monotonous flysch sequence of black shales/schists, metagreywackes, black quartzites and metapsammites interlayered with black siliceous chemiogenic (metacherts/lydites; Pfefferkorn, 1968), presenting maximum deposition age around 540 Ma (e.g. Fernández-Suárez et al., 2002; Linnemann et al., 2008; Pereira et al., 2012a; Schäfer et al., 1993). This unit is similar to Tentúdia succession in Spain.

Locally, the upper *Série Negra* succession presents different designations (Oliveira et al., 1991; Pereira et al., 2006): Mosteiros Formation in Blastomylonitic Belt and Alter do Chão—Elvas Sector, is considered equivalent of Mares Formation in Estremoz Anticline and Águas de Peixe Formation in Montemor—Ficalho Sector (Fig. 1).

The *Série Negra* succession has a distinct tectono-thermal evolution, depending on its location within the OMZ (Eguíluz et al., 2000; Oliveira et al., 1991; Pereira et al., 2006). Indeed, the Variscan metamorphic conditions are heterogeneous along the OMZ, being conditioned by first order tectonic structures (Moreira et al., 2014a). In the Blastomylonitic Belt and Montemor-o-Novo region, the Mosteiros Formation is highly deformed as a result of tectono-metamorphic episodes related to high strain sinistral shear zones during Devonian—Carboniferous times, imposing metamorphism from upper greenschist to amphibolite facies conditions (Chichorro et al., 2008; Pereira et al., 2012b). Otherwise, in the Alter do Chão—Elvas and in the Estremoz Anticline sectors, the metamorphic peak conditions are related to a regional low-grade greenschist facies metamorphism (Moreira et al., 2014b, 2019; Pereira et al., 2012a).

The existing data suggests that the OMZ Ediacaran succession is related to the evolution of the North peri-Gondwana terranes (e.g. Linnemann et al., 2008; Pereira et al., 2006, 2012a). During the Ediacaran, the sedimentary succession of this tectonostratigraphic zone records the inception of a magmatic arc and a corresponding back-arc basin. Hence, the sediments from the top of the *Série Negra* succession are interpreted as originating from the dismantling of this magmatic arc (Linnemann et al., 2008; López-Guijarro, 2006; López-Guijarro et al., 2008; Pereira et al., 2006; Sánchez-Lorda et al., 2014).

3 Sampling and methodology

Representative samples of low to medium-grade black shales from *Série Negra* succession outcropping in the different sectors from OMZ were collected. For sampling, the topmost layer has been removed to avoid the most weathered material. Visual inspection for mineralogical alteration allowed the removal of more altered parts of the samples. Samples ZOM 5, ZOM 6, ZOM 7, ZOM 16 were collected in the Blastomylonitic Belt (Fig. 1B, C), ZOM 12 was collected in the Alter do Chão—Elvas Sector (Fig. 1D), and sample ZOM 15 was collected in the Estremoz Anticline (Fig. 1E). Sample ZOM 16 (collected close to ZOM 6) was collected in the scope of a research project and the geochemical data was used in the present work.

Our data was complemented with previously published data, from other samples from the Ediacaran *Série Negra* succession of the OMZ (Lopes, 2015; Lopes et al., 2015; Pereira et al., 2006) namely the ones that were considered similar and, therefore, were used for comparison purposes. Two samples were described as very fine to fine-grained graphite-rich pelites (SN1 collected in Montemor-Ficalho sector and SN2 collected in the Blastomylonitic Belt, Fig. 1; Pereira et al., 2006). Four samples from Lopes (2015) were identified as metasedimentary lithologies containing graphite (LP1 to LP4 collected in Escoural—Montemor-o-Novo sector, Fig. 1). Pereira et al. (2006) reports that graphite-rich pelites are mainly composed of quartz, phyllosilicates and plagioclase with zircon, chlorite and apatite as accessory minerals. Laranjeira et al. (2023) also described the occurrence of iron oxides in addition to the previous mentioned detrital and metamorphic minerals.

Geochemical analyses from the black shales comprised the determination of the concentration of major, minor and trace elements. In the laboratory, the samples were dried, homogenized, and quartered to get representative portions that were milled to the fractions < 1 mm and < 212 µm. The chemical composition was determined using inductively coupled plasma emission spectrometry/mass spectrometry (ICP-ES/MS) after digestion with an acid solution of H_2O-HF-$HClO_4$-HNO_3, performed at Bureau Veritas Mineral Laboratories (Canada). Analysis of reference materials, duplicates and blanks was performed for quality assurance. The ICP-MS analysis of sample ZOM 16 was carried out in ALS laboratories (Seville, Spain), using the ME-MS81 and ME-4ACD81 analytical packages. Analytical procedures were: (i) Liborate fusion, acid digestion and ICP-MS analysis in

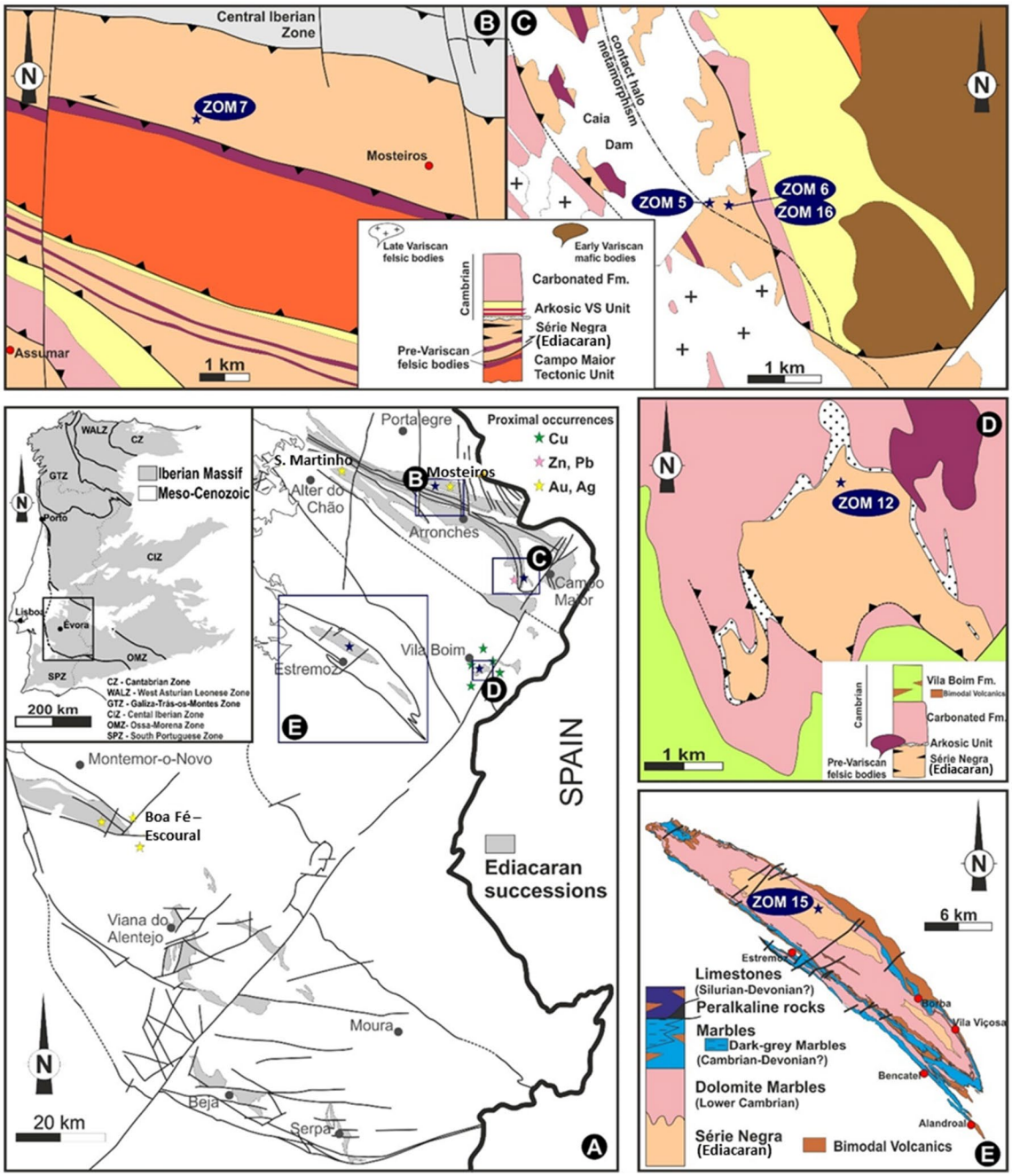

Fig. 1 Geological setting of the studied area and location of samples (adapted from Laranjeira et al., 2023; geological maps adapted from: **A** LNEG, 2010; **B** and **C** LNEG, 2010; Pereira et al., 2010, 2012b; **D** Moreira et al., 2014b; **E** Moreira et al., 2019)

ME-MS81, and (ii) four acid digestion and ICP-AES analysis in ME-4ACD81.

Scanning electron microscopy with energy dispersive X-ray spectrometry (SEM–EDX) analyses were performed to determine qualitative chemical compositions and to identify minerals mode of occurrence. The observations using secondary electrons and backscattered electrons detection modes were made on polished blocks. The SEM–EDX analyses were performed with an FEI Quanta 400FEG environmental scanning electron microscope, equipped with a Genesis X4M energy dispersive X-ray analyser in Materials Centre of the University of Porto.

The chemical composition of black shales was compared with reference materials: Background of Black Shales (BBS; Ketris & Yudovich, 2009), North American Shale Composition (NASC; Condie, 1993; Gromet

et al., 1984; Taylor & McLennan, 1985), Post Archean Australian Shale (PAAS; Condie, 1993; Taylor & McLennan, 1985), Average Shale (AS; Pipper, 1974; Wedepohl, 1971) and Upper Continental Crust (UCC; Rudnick & Gao, 2014). The enrichment/depletion behavior of elements in the studied samples was determined through the calculation of concentration coefficients (CC). Redox sensitive element ratios were used to establish paleoenvironmental conditions (e.g. El-Anwar et al., 2018; Ferreira et al., 2020; Jones & Manning, 1994). Pearson's correlation coefficients were calculated to understand elemental behavior.

4 Results

4.1 Geochemical composition of black shales

Tables 1 and 2 present the geochemical composition of major, minor and trace elements of the studied samples, together with TOC and total sulfur (TS) (Laranjeira et al., 2023), as well as the composition of BBS, NASC, PAAS, AS and UCC for comparison.

The most abundant major and minor elements in the studied samples are Al, Fe, K and Na, followed by smaller amounts of Ca, Mg, P, S and Ti. The chemical composition is consistent with the mineralogical composition described for black shales derived lithotypes of the *Série Negra* (Laranjeira et al., 2023; Pereira et al., 2006).

Aluminum, Fe, K, and Na are the elements that have greater variability amongst the studied samples (Fig. 2). Generally, the samples show a similar pattern, except: (1) sample ZOM 6 that has distinct patterns for Fe, K and Mg content; and (2) sample ZOM 15 that has a notorious higher K content.

The concentration and distribution pattern of selected trace elements is illustrated in Fig. 3. Generally, the elements As, Ba, Be, Co, Cr, Cu, Ga, Hf, Mn, Nb, Ni, Pb, Rb, Sc, Sr, Th, U, Y, V, W, Zn and Zr are found in concentrations above 1 ppm. Elements with concentrations below 1 ppm are Ag, Bi, Cd, In, Ta, Te and Tl. The elements Cs, Mo, Sb, Se and Sn are found in concentrations above and below 1 ppm.

The distribution pattern of the selected elements is quite similar, except for the samples ZOM 6 and ZOM 15. These differences are particularly evident for ZOM 6 sample with lower concentrations of Ba, Cs, ln, Li, Mn, Nb, Rb, and Tl content; whereas the elements Ag, Cd, Cu, Pb, Se, Te and U display higher concentrations (Fig. 3, Tables 1 and 2). Sample ZOM 15 also stands out due to the higher concentrations of As, Ba, Th and ΣLREE (Fig. 3, Tables 1 and 2).

The ΣREE varies from 115 to 330 ppm, with an average value of 194 ppm (Table 2). The REE patterns of the studied samples normalized to BBS (maximum), NASC, PAAS and AS are presented in Fig. 4. The normalized patterns are relatively similar, showing flattened profiles, that are successively less smooth and depleted in heavy REE (HREE) (Fig. 4). This depletion is common in black shales, demonstrating that the patterns were not severely affected by the diagenesis, weathering and metamorphism of the rocks (Boyong et al., 2011). Sample ZOM 7 shows evidence for more differentiated and depleted profiles than the other samples, principally for HREE. Sample ZOM 15 exhibits a more differentiated and enriched profile for light REE (LREE).

In order to compare the geochemical composition of samples with reference values, specifically the BBS (Ketris & Yudovich, 2009), NASC (Condie, 1993; Gromet et al., 1984; Taylor & McLennan, 1985), PAAS (Condie, 1993; Taylor & McLennan, 1985), AS (Pipper, 1974; Wedepohl, 1971) and UCC (Rudnick & Gao, 2014), concentration coefficients (CC) were calculated. The ratio between elements concentration in the samples and their concentration in reference data gives information about the enrichment ($CC > 1$) or depletion ($CC < 1$) of those elements in the studied black shales comparatively to the reference materials. Considering the range for BBS, the CC were calculated considering the maximum values. For REE, the CC were calculated considering the sum of LREE and HREE. Table 3 displays, for each sample, the group of elements having $1 < CC < 2$, $2 < CC < 10$, and $CC > 10$, indicating an increasing degree of enrichment.

The determination of CC reveals that many elements are depleted or have concentration similar to those from the reference materials, being normal ($CC < 1$) to slightly enriched ($1 < CC < 2$) (Table 3). Considering the BBS, only Ba and Th are enriched in sample ZOM 15. For the other reference materials, this is, for NASC, PAAS, AS and UCC, some elements (Ag, As, Cs, Ba, Bi, Cd, Cu, Mo, Pb, Sb, Sn, Se, Th, Tl, U, V, and LREE) generally have $CC > 2$, although Ag, As, Bi, and Se have $CC > 10$ in some samples (mostly ZOM 6 and ZOM 15; Table 3). The elements showing $CC > 10$ are chalcophile elements, with low affinity for oxygen and preferentially bonded with sulfur to form sulfides.

Samples ZOM 6, ZOM 12, and ZOM 15 stand out by their greater number of elements with $CC > 2$ considering all the reference materials, being the majority chalcophile elements. In sample ZOM 6, elements with $CC > 2$ are: Ag, As, Bi, Cd, Cu, Mo, Sb, Se, Pb, and U; the enrichment in Pb was only noticed in this sample. In sample ZOM 12, elements with $CC > 2$ are: As, Bi, Cu, Mo, Sb, Se, U, and V. In sample ZOM 15, the only sample from the Mares Fm., elements with $CC > 2$ are: As, Ba, Bi Sb, Se, Sn, Th, and LREE; the enrichment in Th and LREE was only noticed in this sample. It must be remarked that the samples that contain the most significant enrichment

Table 1 Values of TOC (%), TS (%), concentration of major (wt%), minor (wt%) and trace elements (ppm) in the studied samples and reference values of BBS, NASC, PAAS, AS and UCC for comparison

		Mosteiros Fm					Mares Fm	BBS[1]	NASC[2]	PAAS[3]	AS[4]	UCC[5]
		ZOM 5	ZOM 6	ZOM 7	ZOM 12	ZOM 16	ZOM 15					
TOC*		0.20	1.53	0.29	1.08	n.a	0.76	n.a	n.a	n.a	n.a	n.a
TS*		0.01	0.012	< 0.01	< 0.01	n.a	< 0.01	n.a	n.a	n.a	n.a	n.a
Al	wt%	9.98	5.96	5.97	7.83	n.a	8.26	n.a	16.9	n.a	8.84	15.1
Ca		0.16	0.58	0.17	0.31	n.a	0.16	n.a	3.63	n.a	1.57	3.64
Fe		3.83	0.94	2.71	3.97	n.a	2.35	n.a	5.67	n.a	4.83	4.76
K		2.37	0.11	1.73	2.04	n.a	3.22	n.a	3.97	n.a	2.99	2.76
Mg		0.70	0.08	0.80	0.85	n.a	0.79	n.a	2.86	n.a	1.57	2.45
Na		0.27	2.55	2.12	1.48	n.a	0.93	n.a	1.14	n.a	1.19	3.55
P		0.05	0.03	0.06	0.06	n.a	0.01	0.93–2.20	0.13	n.a	0.07	0.17
Ti		0.54	0.16	0.33	0.49	n.a	0.47	1.50–4.60	0.70	n.a	0.47	0.56
Ag	ppm	0.01	0.40	0.05	0.03	0.25	0.05	0.40–2.40	0.01	0.05	0.07	0.05
As		7.90	18.4	14.6	13.4	9.00	53.3	10.0–80.0	n.a	1.50	10.0	4.80
Ba		769	146	521	636	676	1986	270–800	636	550	580	624
Be		3.00	2.00	2.00	3.00	n.a	2.00	1.00–3.00	n.a	3.00	3.00	2.10
Bi		< 0.04	0.87	< 0.04	0.47	n.a	0.14	0–4.00	0.01	0.13	0.13	0.16
Cd		< 0.02	0.16	< 0.02	< 0.02	0.25	< 0.02	2.00–12.0	0.03	0.10	0.13	0.09
Co		20.5	9.00	10.0	9.70	16.0	4.90	10.0–30.0	26.0	17.0	19.0	17.3
Cr		62.0	37.0	54.0	108	90.0	73.0	50.0–160	125	85.0	90.0	92.0
Cs		12.4	0.20	3.40	1.60	5.77	7.60	2.00–7.00	n.a	4.60	5.50	4.90
Cu		23.1	133	43.6	60.9	27.0	11.4	35.0–150	n.a	25.0	45.0	28.0
Ga		25.1	14.1	13.4	17.8	22.9	27.1	9.00–25.0	n.a	17.0	19.0	17.5
Hf		2.65	3.02	2.90	2.84	5.90	5.38	2.50–6.00	6.30	5.80	2.80	5.30
In		0.06	< 0.01	0.04	0.06	n.a	0.08	n.a	n.a	0.05	n.a	0.06
Li		19.7	3.70	27.1	11.1	30.0	13.2	15.0–50.0	n.a	20.0	n.a	21.0
Mn		366	16.0	275	175	n.a	157	200–800	n.a	n.a	850	n.a
Mo		0.53	6.35	0.30	8.19	0.50	0.33	6.00–60.0	n.a	1.50	2.60	1.10
Nb		16.9	2.34	7.14	15.0	12.5	9.66	7.00–15.0	13.0	12.0	18.0	12.0
Ni		31.8	55.5	31.1	50.5	40.0	22.5	40.0–140	58.0	44.0	68.0	47.0
Pb		4.32	66.3	4.20	7.46	13.0	18.4	10.0–40.0	20.0	17.0	22.0	17.0
Rb		149	2.80	73.5	76.8	111	165	40.0–120	125	112	140	84.0
Sb		0.23	0.42	1.16	1.73	n.a	0.41	0.20–11.0	n.a	0.20	n.a	0.40
Sc		12.1	5.10	7.90	12.1	13.0	16.2	7.00–20.0	15.0	13.6	n.a	14.0
Se		< 0.3	5.80	0.40	< 0.3	n.a	0.40	3.00–30.0	0.08	0.05	0.60	0.09
Sn		3.70	0.60	1.70	2.30	3.00	11.5	2.00–10.0	n.a	5.50	n.a	2.10
Sr		45.0	202	96.0	68.0	138	85.0	100–300	142	350	300	320
Ta		1.30	0.20	0.50	1.10	1.00	0.80	0.50–1.00	1.10	1.00	2.00	0.90
Te		0.07	0.68	0.10	0.17	n.a	0.13	1.30–3.00	n.a	n.a	n.a	n.a
Tl		1.20	< 0.05	0.42	0.34	5.00	0.75	0.50–10.0	n.a	n.a	0.68	0.90
Th		12.1	7.60	6.70	8.10	10.6	26.9	4.00–11.0	12.3	10.7	12.0	10.5
U		2.80	13.3	2.00	5.80	2.91	4.20	4.00–25.0	2.70	2.80	3.70	2.70
Y		11.7	22.6	5.50	18.5	27.5	19.1	15.0–40.0	35.0	22.0	41.0	21.0
V		97.0	147	84.0	284	105	110	100–400	130	107	130	97.0
W		3.20	1.10	1.20	1.80	3.00	3.50	0–15.0	n.a	2.00	n.a	1.90
Zn		40.9	35.1	82.5	33.3	100	33.8	60.0–300	n.a	71.0	95.0	67.0
Zr		80.5	112	97.5	99.4	207	163	60.0–190	200	190	160	193

*Laranjeira et al., 2023; [1]Ketris and Yudovich, 2009; [2]Condie, 1993, Gromet et al., 1984, Taylor & McLennan, 1985; [3]Taylor and McLennan, 1985, Condie, 1993; [4]Wedepohl, 1971, Pipper, 1974; [5]Rudnick and Gao, 2014; n.a—data not available

Table 2 Concentration of REE (ppm) in the studied samples and reference values of BBS, NASC, PAAS, AS and UCC for comparison

	Mosteiros Fm					Mares Fm	BBS[1]	NASC[2]	PAAS[3]	AS[4]	UCC[5]
	ZOM 5	ZOM 6	ZOM 7	ZOM 12	ZOM 16	ZOM 15					
La	31.5	40.1	24.3	31.2	40.1	80.5	20.0–40.0	31.1	38.0	41.0	31.0
Ce	92.4	83.9	51.4	63.0	76.6	145	35.0–80.0	66.7	80.0	83.0	63.0
Pr	8.40	9.90	6.40	8.20	9.34	17.6	2.50–6.00	7.70	8.83	10.1	7.10
Nd	30.5	37.4	21.6	32.0	33.5	58.3	15.0–45.0	27.4	32.0	38.0	27.0
Sm	5.40	7.50	4.30	6.10	6.64	9.70	2.50–7.00	5.59	5.60	7.50	4.70
Eu	1.20	1.70	0.90	1.70	1.21	2.90	1.00–1.40	1.18	1.10	1.61	1.00
Gd	5.20	6.10	3.30	4.40	5.15	6.50	2.50–6.00	4.90	4.70	6.35	4.00
Tb	0.70	0.70	0.40	0.70	0.82	0.70	0.50–0.90	0.85	0.77	1.23	0.70
Dy	3.40	4.30	1.40	4.40	5.19	3.90	1.00–4.00	4.17	4.68	5.50	3.90
Ho	0.50	0.70	0.20	0.70	0.97	0.50	0.20–0.60	1.02	0.99	1.34	0.83
Er	1.30	1.90	0.80	1.90	2.90	1.70	1.00–2.00	2.84	2.85	3.75	2.30
Tm	0.20	0.30	0.10	0.30	0.39	0.40	0.30–0.55	0.84	0.40	0.63	0.30
Yb	1.20	1.90	0.90	2.10	2.86	2.20	2.00–3.50	3.06	2.80	3.53	2.00
Lu	0.20	0.30	0.20	0.30	0.41	0.40	0.30–0.45	0.46	0.43	0.61	0.31
ΣLREE	168	178	107	140	166	311	75.0–178	139	164	180	133
ΣHREE	13.9	17.9	8.20	16.5	19.9	19.2	8.80–19.4	19.3	18.7	24.6	15.3
ΣREE	182	196	115	157	186	330	83.8–197	158	183	204	148
Ce/Ce*	1.30	0.96	0.94	0.90	0.91	0.88	n.a	n.a	n.a	n.a	n.a
Eu/Eu*	1.05	1.17	1.11	1.53	0.96	1.69	n.a	n.a	n.a	n.a	n.a

[1]Ketris and Yudovich, 2009; [2]Condie, 1993, Gromet et al., 1984, Taylor & McLennan, 1985; [3]Taylor and McLennan, 1985, Condie, 1993; [4]Wedepohl, 1971; Pipper, 1974; [5]Rudnick and Gao, 2014; Ce/Ce* Bau & Dulski, 1996; Eu/Eu* Taylor & McLennan, 1985; LREE—light rare earth elements; HREE—heavy rare earth elements; n.a—data not available

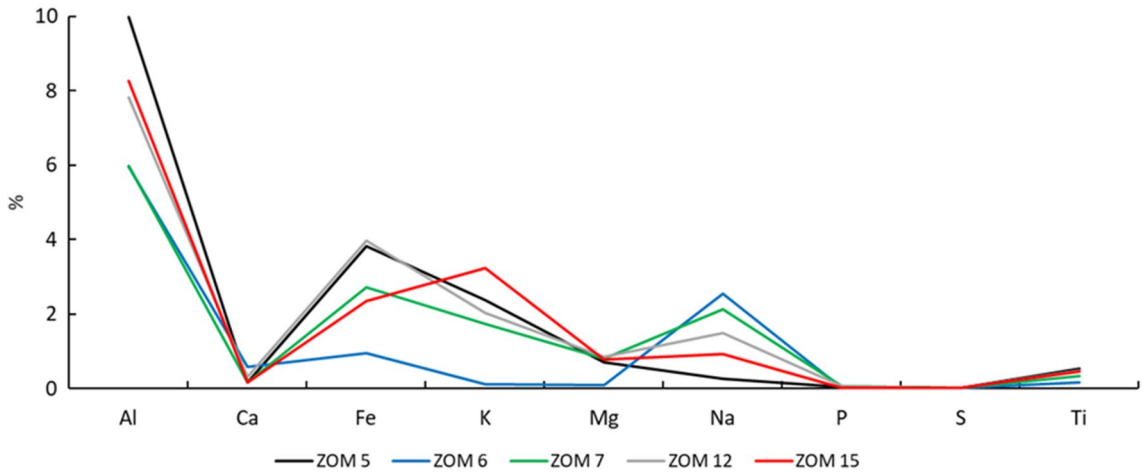

Fig. 2 Concentration of major and minor elements (wt%) in the studied samples

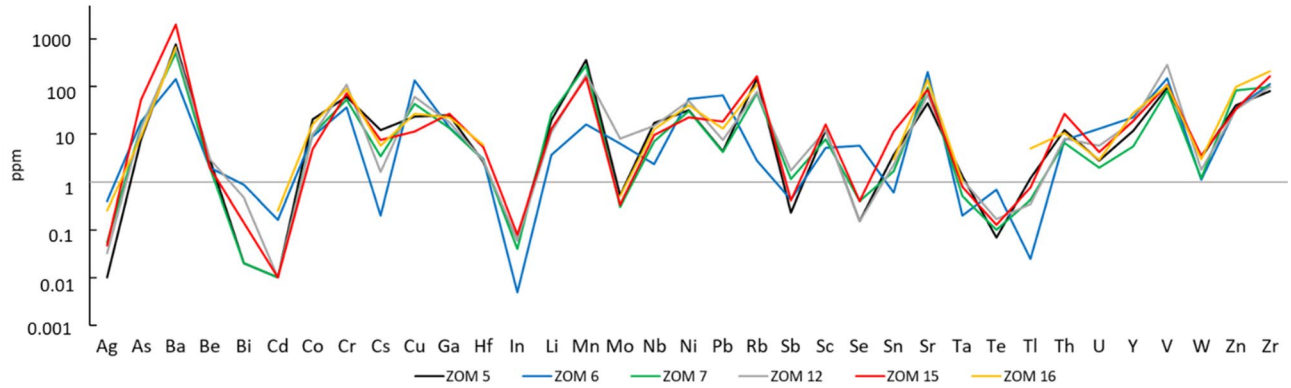

Fig. 3 Concentration of trace elements (ppm) in the studied samples

of trace elements correspond to the samples that have greater TOC content (Table 1).

4.2 Microscopic analysis

The SEM–EDX analyses of the black shales support and provide new insights about their geochemical composition, elemental distribution, and mineralogical content. The SEM–EDX analysis was performed in selected samples (ZOM 6 and ZOM 15). The analyses allow the identification of aluminosilicates, Fe and Ti oxides, and OM in both samples (Figs. 5 and 6). The identified minerals corroborate the previous petrographic observations (Laranjeira et al., 2023). Selected EDX spectra are presented as supplementary material (Figs. S1 and S2).

In the sample ZOM 6, the SEM analysis shows abundant aluminosilicates (Fig. 5, spectrum Z1 in Fig. S1), including some particles occurring in association with Fe oxides (Fig. 5, spectrum Z3 in Fig. S1) and with Ti oxides (Fig. 5, spectrum Z2 in Fig. S1); the detection of inorganic elements from both the aluminosilicates and Fe and Ti oxides in spectra (Fig. 5, spectra Z2 and Z3 in Fig. S1) evidence their association.

In sample ZOM 15, it was also possible to observe the occurrence of aluminosilicates (Fig. 6A, spectra Z1 and Z3 in Fig. S2) in association with Fe, Mn and Ti oxides (Fig. 6A, spectrum Z2 in Fig. S2) and with sulfides, namely arsenopyrite and pyrite (Fig. 6A, respectively spectra Z4 and Z5 in Fig. S2). The observation of Ti oxides in both samples and the significant positive correlation between Fe, Mn and Ti (Table 4) may indicate the presence of ilmenite.

In Fig. 6B it is possible to observe the occurrence of particles exhibiting the association of Fe oxides (Fig. 6B, spectrum Z7 in Fig. S2) with OM (Fig. 6B, spectrum Z6 in Fig. S2) within aluminosilicates (Fig. 6B, spectrum Z8 in Fig. S2). This is supported by the positive correlation coefficients between TOC and some elements preferentially

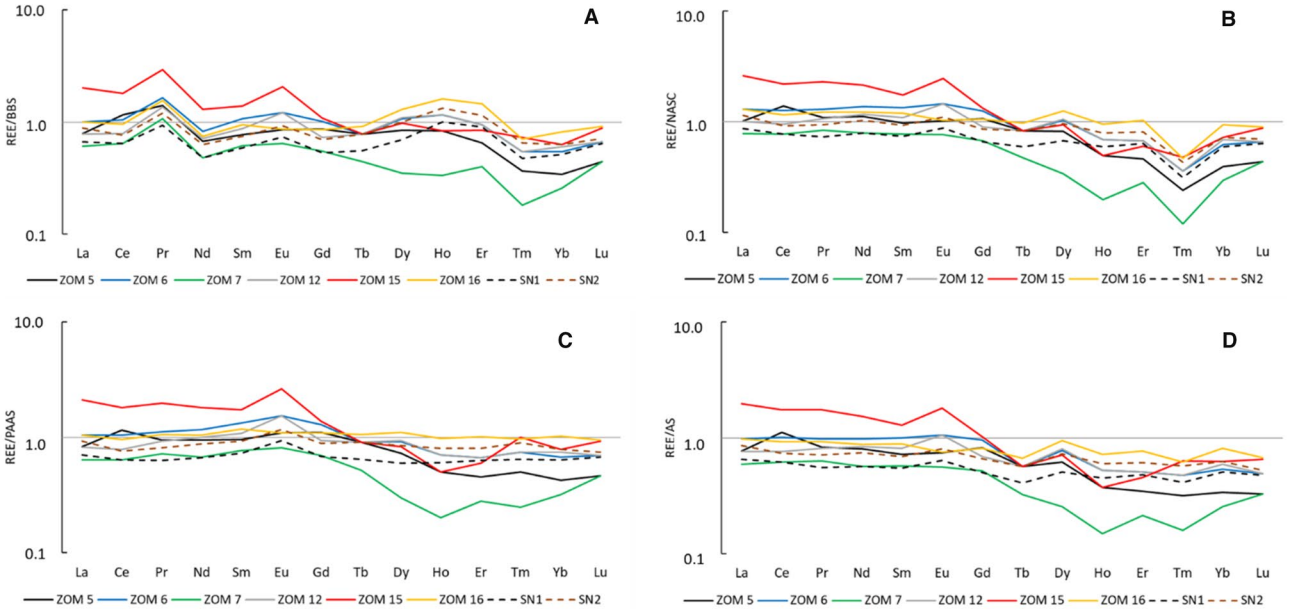

Fig. 4 REE patterns for the studied samples and from graphite-rich pelites from *Série Negra* of OMZ (SN1 and SN2): **A** BBS-normalized REE patterns; **B** NASC-normalized REE patterns; **C** PAAS-normalized REE patterns; and **D** AS-normalized REE patterns

associated with sulfides. The detection of inorganic elements besides C in spectrum Z6 is related to its occurrence within mineral matter.

5 Discussion

5.1 Elemental distribution

The Pearson's correlation coefficients were calculated, and particular attention was given to the enriched elements (CC > 2). Table 4 shows the Pearson's correlation coefficients for selected elements.

The results reveal a significant positive correlation coefficient between TOC and the trace elements Ag, Bi, Cd, Cu, Mo, Ni, Pb, Se, Sr, Te, U, and Y (r > 0.75; Table 4). The association of some of these elements with OM has been already reported in the literature (e.g. El-Anwar et al., 2018; Finkelman et al., 2018; Ribeiro et al., 2019; Ross & Bustin, 2009). However, the preferential affinity of some of them with sulfides is also noticeable. To investigate the sulfides affinity, the correlation coefficients with S was analysed; it was found a weak positive correlation with TOC (r = 0.48) and a strong positive correlation (r > 0.75) with elements normally present in sulfides (Ag, Cd, Cu, Pb, and Se) (El-Anwar et al., 2018; Finkelman et al., 2018). Therefore, Ag, Cd, Cu, Pb and Se are thought to be preferentially associated with sulfides, whereas the elements Mo and U might be preferentially organically bound.

The moderate positive correlation between TOC and S indicates the occurrence of sulfides in association with OM, which corroborates the previous petrographic characterization of these samples (Laranjeira et al., 2023). The petrography revealed the occurrence of OM associated with iron oxides, including oxidized pyrite, and other sulfides. Iron displays positive correlation with Al, Ti and Mn, which indicates its association with aluminosilicates and oxides. In addition, for the referred elements, Ag, Bi, Cd, Cu, Mo, Pb, and Se they present CC > 2 in the studied black shales comparatively to reference materials (except BBS), reinforcing their importance in the studied samples, and the importance of the occurrence of OM in association with sulfides and oxides.

Most of the other elements have a negative correlation with TOC and a positive correlation with Al, pointing out their association with aluminosilicates (El-Anwar et al., 2018; Finkelman et al., 2018). These include, among others, Ba, Sn, Th, Tl, and LREE, which also have CC > 2.

5.2 Sedimentary sources and geochemical proxies of paleo-redox environments

The geochemical discriminant diagrams (Bhatia & Crook, 1986; Floyd & Leveridge, 1987) show that the clastic compounds of black shales derived essentially from a Continental Island Arc source (Fig. 7A and B), with acidic to mixed felsic/basic signatures (Fig. 7C). This data is consistent with the one obtained in previous works for diverse lithotypes including metamorphosed greywackes and shales,

Table 3 Concentration coefficients (CC) of trace elements in the studied samples relatively to BBS, NASC, PAAS, AS and UCC

Samples	1 < CC < 2	2 < CC < 10	CC > 10
BBS			
ZOM 5	Cs, Nb, Rb, Ta, Th		
ZOM 6	Pb		
ZOM 7			
ZOM 12	Ta		
ZOM 15	Cs, Ga, Rb, Sn, LREE	Ba, Th	
ZOM 16	Zr, HREE		
NASC			
ZOM 5	Ba, Nb, Rb, Se, Ta, U, LREE	Bi	
ZOM 6	Sr, V, LREE	Cd, Pb, U	Ag, Bi, Se
ZOM 7		Ag, Bi, Se	
ZOM 12	Nb, Se, LREE	Ag, U, V	Bi
ZOM 15	Rb, Sc, U	Ag, Ba, Se, Th, LREE	Bi
ZOM 16	Ba, U, Zr, LREE, HREE	Cd	Ag
PAAS			
ZOM 5	Ba, Co, Ga, ln, Nb, Rb, Sb, Ta, Th, W, LREE	As, Cs, Se	
ZOM 6	Cd, Ni, Y, V, LREE, HREE	Ag, Bi, Cu, Mo, Pb, Sb, U	As, Se
ZOM 7	Ag, Cu, Li, Zn	As, Sb, Se	
ZOM 12	Ba, Cr, Ga, ln, Nb, Ni, Ta, LREE, HREE	As, Bi, Cu, Mo, Sb, Se, U, V	
ZOM 15	Bi, Cs, Ga, ln, Pb, Rb, Sc, U, V, W, HREE	Ba, Sb, Se, Sn, Th, LREE	As
ZOM 16	Ba, Cr, Cs, Cu, Ga, Hf, Li, Nb, U, Y, W, Zn, Zr, LREE, HREE	Ag, As, Cd	
AS			
ZOM 5	Ba, Co, Ga, Rb, Tl, Th	Cs	
ZOM 6	As, Cd, Hf, V	Ag, Bi, Cu, Mo, Pb, Se, U	
ZOM 7	As, Hf		
ZOM 12	As, Ba, Cr, Cu, Hf, U	Bi, Mo, V	
ZOM 15	Bi, Cs, Ga, Hf, Rb, Tl, U, Zr, LREE	As, Ba, Th	
ZOM 16	Ba, Cd, Cs, Ga, Zn, Zr	Ag, Hf, Tl	
UCC			
ZOM 5	As, Ba, Be, Co, Ga, ln, Nb, Rb, Se, Sn, Ta, Tl, U, W, LREE	Cs	
ZOM 6	Cd, Ni, Sb, Y, V, LREE, HREE	Ag, As, Bi, Cu, Mo, Pb, U	Se
ZOM 7	Ag, Cu, Li, Zn	As, Sb, Se	
ZOM 12	Ba, Be, Cr, Ga, ln, Nb, Ni, Se, Sn, Ta, LREE, HREE	As, Bi, Cu, Mo, Sb, U, V	
ZOM 15	Cs, Ga, Hf, ln, Pb, Rb, Sb, Sc, U, V, W, HREE	Ba, Se, Sn, Th, LREE	As
ZOM 16	As, Ba, Cs, Ga, Hf, Li, Nb, Rb, Sn, Ta, Th, U, Y, V, W, Zn, Zr, LREE, HREE	Ag, Cd, Tl	

as well as para-derived high temperature lithotypes from *Série Negra* succession (Lopes, 2015; López-Guijarro, 2006; Lopes et al., 2015; Pereira et al., 2006). This data is also in accordance with the main geodynamic model proposed for the evolution of OMZ, which indicates the development of magmatic-arc and related back-arc basin in the North Gondwana realm, where the OMZ was located, during late Ediacaran times (e.g. Chichorro et al., 2008; Linnemann et al., 2008; Pereira et al., 2006; Sánchez-Lorda et al., 2014).

The ratio between some trace elements (e.g. Co, Cr, Cu, Mo, Ni, Th, U, V, Zn) has also been used as proxies for evaluation of redox depositional conditions during the sedimentary processes (e.g. Arning et al., 2009; El-Anwar et al., 2018; Ferreira et al., 2020; Jones & Manning, 1994; Pi et al., 2013). The ratios V/Cr, Ni/Co, U/Th and (Cu + Mo)/Zn, whose values increase under anoxic conditions, were calculated. Complementarily, TOC/Al and U/Mo for the studied samples were also determined and are all presented in Table 5.

The ratio V/Cr in samples ZOM 6 (3.97) and ZOM 12 (2.63) indicate anoxic conditions, while the other values, ranging from 1.17 to 1.56, point to more oxidizing conditions (according to Jones & Manning, 1994, values of the ratio V/Cr above 2 indicate anoxic depositional conditions).

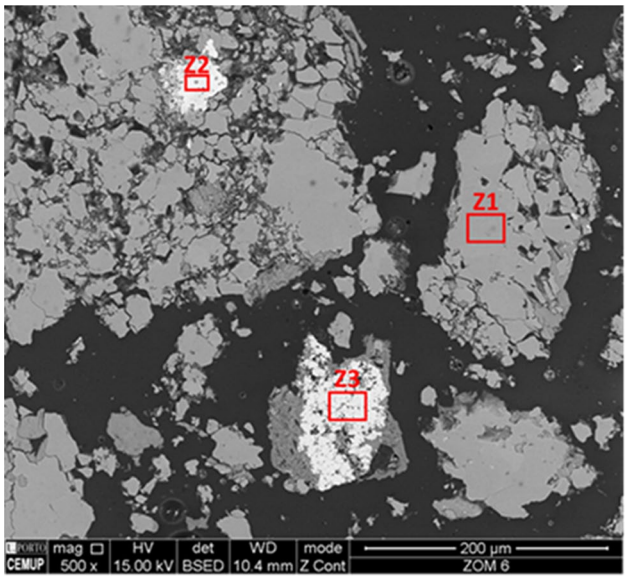

Fig. 5 SEM image of aluminosilicates (Z1), titanium oxides and associated aluminosilicates (Z2), and iron oxides and associated mineral matter (Z3) in sample ZOM 6. The spectra of EDX analysis of Z1 to Z3 are presented in Fig. S1

Samples ZOM 6 and ZOM 12 present the higher V concentrations (147 ppm and 284 ppm, respectively), which indicate a V enrichment in these samples compared with reference materials (except the maximum for BBS) and supports the fact that V is more concentrated in sediments deposited under reducing conditions (e.g. Emerson & Huested, 1991; Jones & Manning, 1994; Shaw et al., 1990). Similar paleo-redox conditions are also emphasized by the ratio (Cu + Mo)/Zn, indicator of the oxygenation of bottom waters (Hallberg, 1976, 1982), which show higher ratio values in samples ZOM 6 (3.97) and ZOM 12 (2.07).

The high values of Ni/Co ratio show similar behavior for samples ZOM 6 and ZOM 12, including the sample ZOM 15 (Table 5) on samples that emphasize stronger reducing conditions during depositional processes (e.g. Dill, 1986; Dypvik, 1984; Jones & Manning, 1994). Tribovillard et al. (2006) suggested that the presence of Ni can be used as a proxy for primary paleoproductivity due to its accumulation in organic-rich sediments, which is also in accordance with the CC between TOC and Ni (Table 4).

The ratio U/Th is also usually used as a redox indicator (e.g. Adams & Weaver, 1958; Roger and Adams, 1969 *in* Jones & Manning, 1994; Ferreira et al., 2020). The increase of U/Th ratio is expected with the increase of anoxic conditions due to the accumulation of authigenic U in organic sediments,that is enhanced during deposition under progressively greater oxygen depletion (Ferreira et al., 2020). Indeed, the projection of U/Th and V/Cr ratios (Fig. 8) reveals that sample ZOM 6 is associated with anoxic conditions (similar to BBS) and sample ZOM 12 is associated with a suboxic domain. The other samples and reference materials are projected in the oxic conditions field, as well as organic-rich pelites of Pereira et al. (2006) and metasedimentary lithologies with graphite from Lopes (2015).

The ratio U/Mo has also been used to differentiate between anoxic non-sulfidic and anoxic sulfidic conditions (Arning et al., 2009). The lowest values of U/Mo were

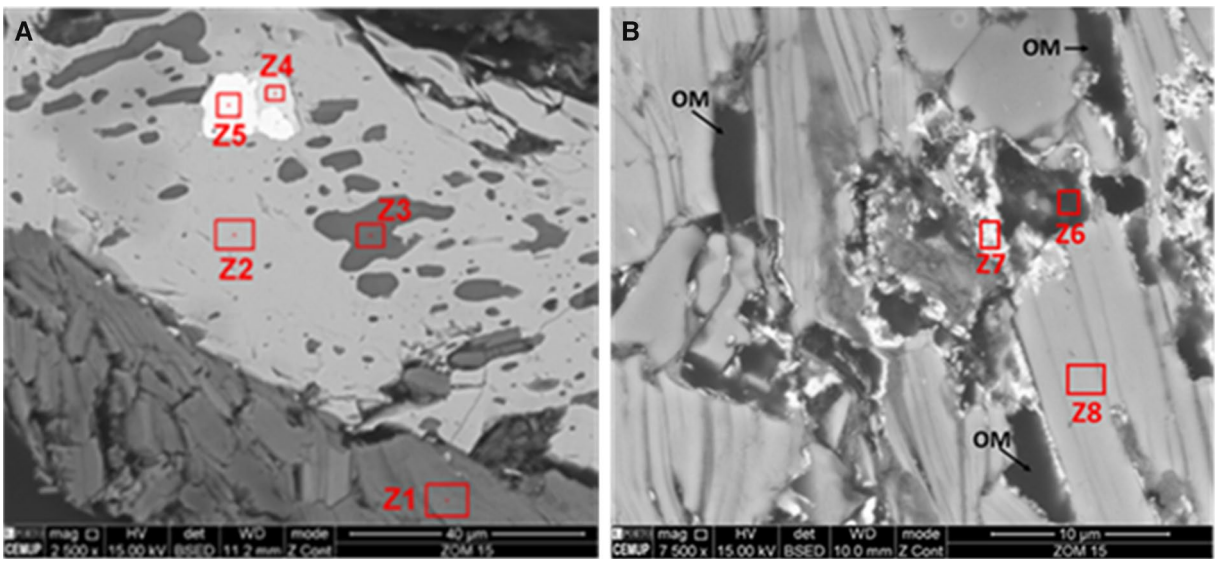

Fig. 6 SEM images of: **A** aluminosilicates (Z1 and Z3) and associated mineral matter, titanium oxide (Z2), pyrite (Z4) and arsenopyrite (Z5) in sample ZOM 15; **B** organic matter and associated mineral matter (principally aluminosilicates) (Z6), iron oxides and associated aluminosilicates (Z7) and aluminosilicates (Z8) in sample ZOM 15. The spectra of EDX analysis of Z1 to Z8 are presented in Fig. S2

Table 4 Pearson's correlation coefficients of selected elements

	TOC	S	Al	Fe	Ti	Ag	As	Bi	Cd	Cu	Mn	Mo	Ni	Pb	Sb	Se	Te	U	Y	V
TOC																				
S	0.48																			
Al	-0.47	-0.15																		
Fe	-0.58	-0.58	0.67																	
Ti	-0.61	-0.61	**0.87**	**0.88**																
Ag	**0.77**	**0.83**	-0.61	**-0.87**	**-0.91**															
As	0.15	-0.31	0.03	-0.35	0.07	-0.04														
Bi	**0.96**	0.65	-0.49	-0.58	-0.69	**0.86**	-0.09													
Cd	**0.76**	**0.88**	-0.54	**-0.82**	**-0.87**	**0.99**	-0.10	**0.86**												
Cu	**0.80**	**0.74**	-0.66	-0.64	**-0.85**	**0.92**	-0.33	**0.92**	**0.92**											
Mn	**-0.95**	-0.41	0.60	**0.76**	0.71	**-0.81**	-0.35	**-0.88**	**-0.77**	-0.74										
Mo	**0.81**	0.28	-0.29	-0.07	-0.31	0.45	-0.31	**0.83**	0.47	0.71	-0.62									
Ni	**0.78**	0.56	-0.42	-0.24	-0.54	0.66	-0.51	**0.89**	0.69	**0.89**	-0.60	**0.92**								
Pb	**0.82**	**0.81**	-0.51	**-0.88**	**-0.83**	**0.98**	0.12	**0.86**	**0.98**	**0.85**	**-0.85**	0.43	0.60							
Sb	0.11	-0.57	-0.32	0.43	0.10	-0.29	-0.29	0.07	-0.33	0.06	-0.01	0.52	0.34	-0.38						
Se	**0.76**	**0.86**	-0.57	**-0.85**	**-0.88**	**1.00**	-0.06	**0.85**	**1.00**	**0.91**	**-0.78**	0.44	0.66	**0.98**	-0.33					
Te	**0.85**	**0.81**	-0.57	**-0.81**	**-0.86**	**0.99**	-0.06	**0.92**	**0.99**	**0.94**	**-0.85**	0.57	0.74	**0.98**	-0.22	**0.99**				
U	**0.92**	**0.77**	-0.47	-0.72	**-0.75**	**0.94**	-0.02	**0.97**	**0.95**	**0.91**	**-0.88**	0.68	**0.79**	**0.95**	-0.16	**0.94**	**0.98**			
Y	**0.87**	0.43	-0.03	-0.42	-0.26	0.57	0.38	**0.78**	0.58	0.50	**-0.81**	0.63	0.52	0.70	-0.16	0.57	0.66	**0.78**		
V	0.56	-0.14	-0.02	0.32	0.12	0.00	-0.20	0.51	0.02	0.30	-0.35	**0.89**	0.66	0.01	0.71	-0.01	0.14	0.30	0.49	

Strong positive correlations (> 0.75) are identified in blue, and strong negative correlations are marked in red (> − 0.75)

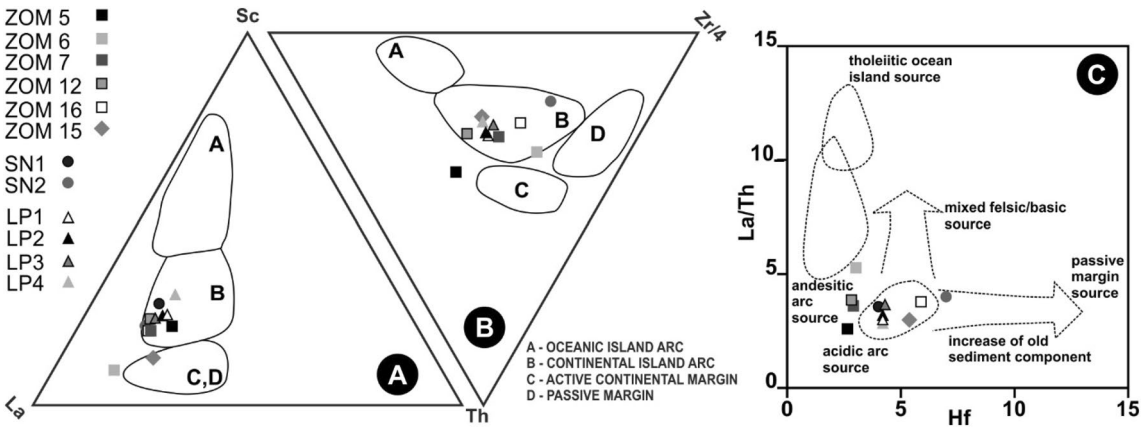

Fig. 7 **A** Ternary La-Th-Sc diagram adapted from Bhatia and Crook (1986); **B** Ternary Th-Sc-Zr/4 diagram adapted from Bhatia and Crook (1986) and **C** La/Th-Hf diagram from Floyd and Leveridge (1987)

Table 5 Ratio of selected redox sensitive elements for the studied samples

	ZOM 5	ZOM 6	ZOM 7	ZOM 12	ZOM 15	ZOM 16
V/Cr	1.56	3.97	1.56	2.63	1.51	1.17
Ni/Co	1.55	6.17	3.11	5.21	4.59	2.50
U/Th	0.23	1.75	0.30	0.72	0.16	0.27
U/Mo	5.28	2.09	6.67	0.71	12.7	5.82
(Cu + Mo)/Zn	0.58	3.97	0.53	2.07	0.35	0.28
TOC/Al	0.02	0.26	0.05	0.14	0.09	–

obtained for samples ZOM 6 (2.09) and ZOM 12 (0.71), resulting from highest Mo concentration in this samples and, therefore, indicating that were deposited under more anoxic sulfidic conditions (Algeo & Lyons, 2006; Algeo & Maynard, 2004). This is also supported by the higher concentration of elements with affinity with sulfides on sample ZOM 6.

The Eu and Ce anomalies are also important proxies because these elements are sensitive to changes in redox conditions due to their different behaviour when compared to other REE (Leybourne et al., 2000):

– The normalized patterns reveal a positive Eu anomaly for almost all samples (Eu/Eu* = 0.96–1.69, average 1.25; Table 2; Fig. 4). The higher Eu positive anomalies in

samples ZOM 6, ZOM 12 and ZOM 15 could be related either with the presence of detrital plagioclase and/or the anoxic conditions during depositional processes.

– The Ce negative anomaly was identified as a consequence of the change in the oxidation state of Ce (Elderfield & Greaves, 1982) and can also be used as an indicator of intensity of anoxia depending on the depositional setting (e.g. Murray et al., 1990; Wilde et al., 1996). Only the sample ZOM 5 shows a positive Ce anomaly (Ce/Ce* = 1.30), while the remaining samples have slightly negative anomalies (Ce/Ce* = 0.88–0.96) (Table 2; Fig. 4), which may reflect less reducing conditions in sample ZOM 5.

Interrelating the Eu and Ce anomalies (Fig. 9), samples ZOM 16 and ZOM 5 seem to be related to more oxidizing environments, while the other samples seem to be deposited in more reducing depositional conditions (Fig. 9).

All the used ratios (Table 5), as well as the Ce and Eu anomalies, revealed that the samples ZOM 6 and ZOM 12, and secondarily the sample ZOM 15, were deposited under anoxic conditions, while the other samples were deposited in more oxidizing conditions, although with dissimilar paleoredox conditions. This is consistent with the TOC values that are higher in ZOM 6 and ZOM 12, in which the redox conditions favored the OM preservation, and the increase of some redox sensitive elements (e.g. Mo, U, V). Samples ZOM 5, ZOM 7 and ZOM 15 behave consistently presenting lower TOC values (< 1%), and redox sensitive proxies pointing to more oxic to suboxic depositional conditions. The same pattern was found for organic-rich pelites and metasedimentary lithologies with graphite from the *Série Negra* of OMZ (Lopes, 2015; Pereira et al., 2006).

Therefore, the *Série Negra* succession can be interpreted as related to the erosion of the Cadomian magmatic-arc, being deposited in proximal back-arc basin. The geochemical composition of black shales from this succession indicates discrepant anoxic conditions, which can be interpreted as resulting from the variation of paleoredox conditions within the back-arc basin generated during the last episodes of the magmatic-arc inception.

5.3 Série Negra as possible source of metals

The diversity of ore deposits and mineral occurrences in OMZ result from a complex tectono-metamorphic evolution derived from the location of the OMZ within Iberian Massif and the existence of several magmatic-hydrothermal events during the Cadomian and Variscan Cycles (Liñán & Quesada, 1990; Tornos et al., 2004).

The tectono-metamorphic, magmatic and depositional processes have certainly controlled the genesis of many ore deposits in OMZ (Tornos et al., 2002). Indeed, the OMZ is characterized by significant crustal heterogeneities (Locutura et al., 1990), which imposes variations in the composition of the metal reservoir, and the multiple tectono-metamorphic and magmatic-hydrothermal processes that might have conditioned the transport and precipitation of the metals (Tornos et al., 2004), thus reflecting the differences between the metallogenic belts within this tectonostratigraphic domain. Therefore, the OMZ displays a great variety of ore occurrences, including Fe, Pb–Zn, Cu, Au, Ag, Sb, Ni, Mn, W, Hg, U and REE, among others, which are

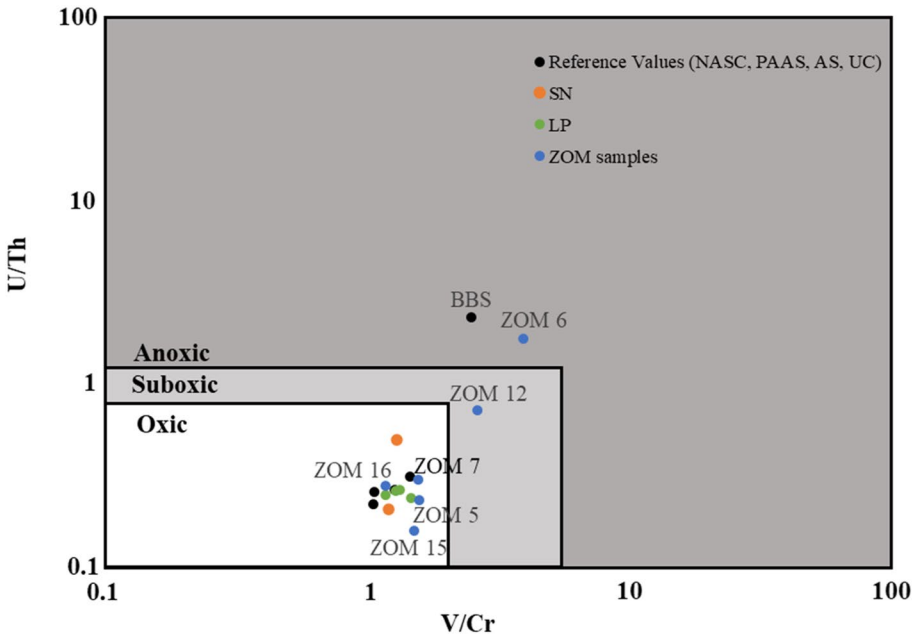

Fig. 8 Cross plot of redox-sensitive trace elements ratios (U/Th versus V/Cr; adapted from Piercey et al., 2016) of the studied samples and reference materials for comparison. SN—samples from Pereira et al. (2006); LP—samples from Lopes (2015); BBS (Ketris & Yudovich, 2009); NASC (Condie, 1993; Gromet et al., 1984; Taylor & McLennan, 1985); PAAS (Condie, 1993; Taylor & McLennan, 1985); AS (Pipper, 1974; Wedepohl, 1971) and UCC (Rudnick & Gao, 2014)

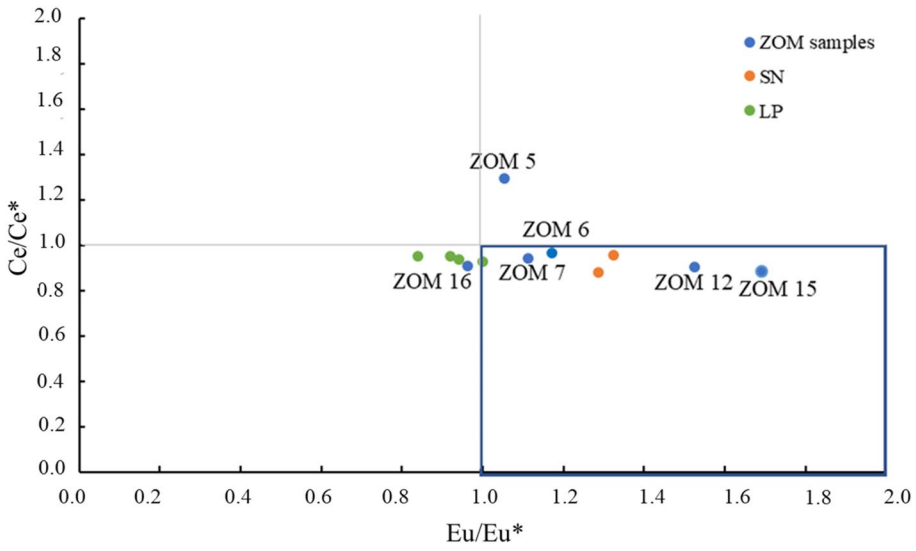

Fig. 9 Ce/Ce* and Eu/Eu* cross plot considering the studied samples and from samples of *Série Negra* of OMZ studied by Pereira et al. (2006) and Lopes (2015) containing graphite (SN and LP, respectively). The highlighted field represents a more reducing depositional conditions

formed by different processes in distinct geological settings and times (Tornos et al., 2004).

Some Au occurrences are reported in OMZ (Fig. 1A), namely in the Arronches-Córdoba Belt (Mosteiros—Nave de Grou and São Martinho—Blastomylonitic Belt), Évora—Aracena Belt (Boa Fé-Escoural), and in the Olivenza—Monesterio Belt (Guijarro and Chocolatero) (Canales & Matas, 1992; Matos & Filipe, 2013; Tornos et al., 2004). These occurrences are considered as orogenic Au deposits, controlled by major shear zones. They are characterized by sulfide-poor quartz-bearing veins, breccias and disseminations in a host-rock, and have been interpreted as Variscan syn-metamorphic mineralizations (Maia et al., 2022; Oliveira et al., 2007; Tornos et al., 2004).

In Alter do Chão—Elvas and Estremoz Anticline Sectors (Central Belt), several Cu mineralizations are present (Matos & Filipe, 2013), most of these mineralizations are interpreted as late Variscan Cu-Veins (Maia et al., 2020; Mateus et al., 2013) hosted in Paleozoic successions. In the North—Central Belt (Alter do Chão—Elvas sector) most of Cu, Zn and Pb occurrences are hosted in Lower Cambrian Succession (Mateus et al., 2013; Oliveira, 1986), being concurrently described some Au and Ag enrichments in similar occurrences in Spain (Tornos et al., 2004).

Figure 10 shows the enrichment of selected elements that may have affinity with Au, Pb, Zn and Cu, namely, Ag, As, Bi, Cd, Co, Cr, Mo, Ni, Sb, Se, U and V (Huyck, 1989; Large et al., 2011). Although the Au content was not analyzed in the studied samples, several elements have a geochemical affinity with Au, and can be used as proxies to discuss the potential presence of Au. All samples present a significant enrichment in As and Se, both with strong affinity with Au (Large et al., 2011). Samples ZOM 6 and ZOM 12, with higher TOC, also shows significant enrichment in Bi and Mo, in addition to Ag and Cu on sample ZOM 6 and Sb on sample ZOM 12. The presence and relative enrichment of these elements in the mentioned samples could be indicative of primary presence of Au. Furthermore, samples ZOM 6 and ZOM 12 are associated with anoxic to suboxic environments, which favor the formation of significant amounts of diagenetic pyrite (Large et al., 2011; Tribovillard et al., 2006), although diagenetic pyrite can form in a wide range of conditions. It is noteworthy that the petrographic and SEM observations (Laranjeira et al., 2023) reveal the presence of pyrite crystals in sample ZOM 6.

Previous studies on OM-rich sediments showed that some Au deposits have a strong positive correlation with As and S contents (Large et al., 2011). In reduced continental margin basin settings, the OM-rich sediments deposited under anoxic to euxinic conditions concentrate Au, As, S, and other trace elements such as Ag, Cu, Mo, Ni, Se, Te, V, U, and Zn in pyrite and arsenopyrite phases (Large et al., 2011; Tribovillard et al., 2006).

It is plausible that successive tectono-metamorphic processes, namely the Variscan shear zones, could remobilize Au, As, S and other elements (e.g. Bi, Cu, Mo, Pb, Sb, Te, Tl and Zn) from these OM-rich sediments to become concentrated by hydrothermal processes (Large et al., 2011).

Indeed, Tornos et al. (2004) suggest that OMZ orogenic Au mineralizations were probably formed by hydrothermal/metamorphic fluids that leached Au contained in the *Série Negra* succession, in accordance with recent data from Maia et al. (2022) which suggest that the Neoproterozoic metasediments were the most probable suppliers of S and Au to the system. Therefore, the hydrothermal/metamorphic fluids related to Variscan transpressional shear zones may remobilize the Au content within black shales from *Serie Negra* succession, thus enabling the genesis of quartz-bearing veins and stockworks with a possible enrichment in Au. However, it must be emphasized that not all *Serie Negra* succession

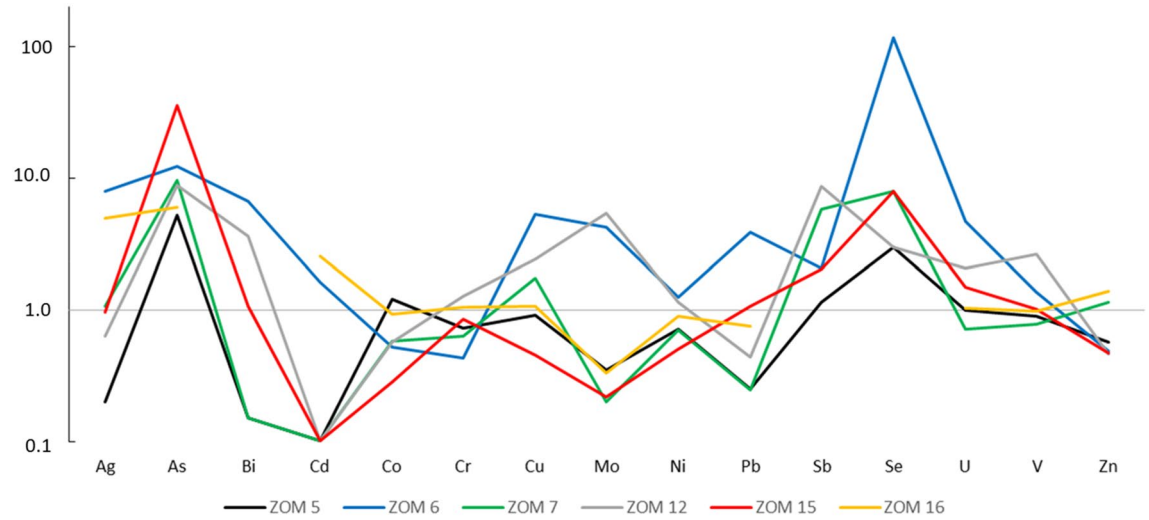

Fig. 10 Selected elements with possible affinity with Au, Pb, Zn and Cu normalized to PAAS (Condie, 1993; Taylor & McLennan, 1985)

lithotypes have a propensity to be an Au source. Indeed, only the black shales deposited in most anoxic environments (ZOM 6 and ZOM 12) seem to show an increase of content in elements with significant Au geochemical affinity.

If it is considered that the black shales of the *Série Negra* succession have a primary Au content, the depleted pattern of some samples (e.g. ZOM 7) may be interpreted as related to the remobilization of metals during Tomar—Badajoz—Córdoba shear events (Pereira et al., 2010, 2012b). Those remobilized metals may be focused, and the shear zone activity may form extensional structures, that allowed the precipitation of metals and, consequently, the genesis of some Au occurrences in the OMZ high grade domains (e.g. Montemor-o-Novo region and Blastomylonitic Belt).

Near the location where samples ZOM 5, ZOM 6 and ZOM 16 were collected, an occurrence of Pb–Zn is known, possibly related to late hydrothermal processes associated with the emplacement of Santa Eulália Plutonic Complex (Fig. 1A). This fact may explain the enrichment in Pb content in sample ZOM 6 relatively to the remaining samples. However, this increase could also be primary, because the other samples from this location (ZOM 5 and ZOM 16) do not show similar behavior.

Sample ZOM 12 is located near some Cu occurrences (Fig. 1A). According to what was previously demonstrated by the paleoredox ratios, sample ZOM 12 corresponds to suboxic to anoxic paleoenvironmental conditions and has a significant enrichment in Ag, As, Bi, Cu, Mo, Sb, Se, U and V (Table 3; Fig. 10). The positive correlations between TOC and some redox-sensitive elements, and specifically with Cu ($r = 0.80$) corroborates their formation and Cu enrichment formed under suboxic to anoxic conditions.

6 Conclusions

Black shales from *Série Negra* succession of OMZ were studied using a geochemical and mineralogical approach to trace the depositional paleoenvironments and the possible sources based on redox sensitive elements. The results indicate that the metal occurrences on OMZ and the black shales from *Série Negra* succession seems to be linked.

The clastic sources of the studied black shales are related with the dismantling of the Cadomian Continental Arc developed in the North Gondwana margin, showing acidic to mixed felsic/basic signatures, which is in accordance with previous proposed models.

The CC considering different reference materials reveal an enrichment ($CC > 2$) in several elements: Ag, As, Cs, Ba, Bi, Cd, Cu, Mo, Pb, Sb, Sn, Se, Th, Tl, U, V, and LREE. Samples ZOM 6, ZOM 12, and ZOM 15 have the high number of enriched elements. Some samples reveal $CC > 10$ for Ag, As, Bi, and Se. Based on Pearson's correlation coefficient and considering the significant positive correlations between TOC and S, it is demonstrated the association of OM with the occurrence of sulfides, corroborating the petrographic description of the samples. The elements Ag, Cd, Cu, Pb and Se are thought to be preferentially associated with sulfides, while the elements Mo and U must be preferentially organically bound. The Eu positive anomaly, the Ce negative anomaly and the ratios calculated based on redox sensitive elements indicate oxic to anoxic paleoenvironmental conditions, being more noticeable the anoxic conditions in samples ZOM 6 and ZOM 12, which are also the samples with highest TOC values. Those samples are enriched in Ag, As, Bi, Co, Cu, Mo, Sb and Se indicating that the BS deposited

in anoxic environment and may represent an important source of metals as proposed by other authors.

Supplementary Information The online version contains supplementary material available at https://doi.org/10.1007/s41513-022-00202-6.

Acknowledgements This work is supported by national funding awarded by FCT—Foundation for Science and Technology, I.P., projects UIDB/04683/2020 and UIDP/04683/2020. V. Laranjeira thanks the funding of the PhD scholarship (SFRH / BD / 137567/2018) awarded by FCT and the EU, through national funds and the European Social Fund (ESF). N. Moreira and P. Nogueira acknowledge the contribution of the project ZOM-3D (ALT20-03-0145-FEDER-000028), funded by Alentejo 2020 through the FEDER/FSE/FEEI. The authors acknowledge J. Roseiro for the English editing.

Funding Open access funding provided by FCT|FCCN (b-on).

Data Availability The authors declare that the data supporting the findings of this study are available within the article and its supplementary information files.

Declarations

Conflict of interest The authors declare that do not have conflicts of interest.

References

Adams, J. A. S., & Weaver, C. E. (1958). Thorium to uranium ratios as indicators of sedimentary processes-Examples of the concept of geochemical facies. *American Association of Petroleum Geologists Bulletin, 42*, 387–430.

Ai, J. Y., George, S. C., & Zhonga, N. N. (2020). Organic geochemical characteristics of highly mature Late Neoproterozoic black shales from South China: Reappraisal of syngeneity and indigeneity of hydrocarbon biomarkers. *Precambrian Research, 336*, 105508. https://doi.org/10.1016/j.precamres.2019.105508

Algeo, T. J., & Lyons, T. W. (2006). Mo-total organic carbon covariation in modern anoxic marine environments: implications for analysis of paleoredox and paleohydrographic conditions. *Paleoceanography*. https://doi.org/10.1029/2004PA001112

Algeo, T. J., & Maynard, J. B. (2004). Trace-element behavior and redox facies in core shales of Upper Pennsylvanian Kansas-type cyclothems. *Chemical Geology, 206*, 289–318. https://doi.org/10.1016/j.chemgeo.2003.12.009

Alía, M. (1963). Rasgos estructurales de la Baja Extremadura. *Boletín Real Sociedad Española Historia Natural (geología), 20*, 247–262.

Apalategui, O., Eguíluz, L., & Quesada, C. (1990). Ossa-Morena zone: structure. In R. D. Dallmeyer & E. Martínez-García (Eds.), *Pre-Mesozoic Geology of Iberia* (pp. 280–292). Springer-Verlag.

Araújo, A., Piçarra de Almeida, J., Borrego, J., Pedro, J., & Oliveira, J. T. (2013). As Regiões Central e sul da Zona de Ossa Morena. In R. Dias, A. Araújo, P. Terrinha, & J. C. Kullberg (Eds.), *Geologia de Portugal* (Vol. I, pp. 509–549). Geologia Pré-mesozóica de Portugal, Escolar Editora.

Arning, E. T., Lückge, A., Breuer, C., Gussone, N., Birgel, D., & Peckmann, J. (2009). Genesis of phosphorite crusts off Peru. *Marine Geology, 262*, 68–81. https://doi.org/10.1016/j.margeo.2009.03.006

Bau, M., & Dulski, P. (1996). Distribution of yttrium and rare-earth elements in the Penge and Kuruman iron-formations, Transvaal Supergroup, South Africa. *Precambrian Research, 79*(1–2), 37–55. https://doi.org/10.1016/0301-9268(95)00087-9

Bhatia, M. R., & Crook, K. A. (1986). Trace element characteristics of graywackes and tectonic setting discrimination of sedimentary basins. *Contributions to Mineralogy and Petrology, 92*(2), 181–193. https://doi.org/10.1007/BF00375292

Boyong, Y., Bin, H., Zhengyu, B., & Zhaogan, Z. (2011). REE geochemical characteristics and depositional environment of the black shale-hosted Baiguoyuan Ag-V deposit in Xingshan, Hubei Province, China. *Journal of Rare Earths, 29*(5), 499–506.

Canales, A., & Matas, J. (1992). Anomalías de Au en el flanco Sur del Anticlinorio de Olivenza-Monesterio. In I. Rábano, & J. C. Gutierrez Marco (Eds.), *Libro de Resúmenes* (53 p.). VIII Reunión de Ossa Morena.

Carvalhosa, A. (1965). Contribuição para o conhecimento geológico da região entre Portel e Ficalho (Alentejo). *Memorias Dos Serviços Geológicos De Portugal, 11*, 1–130.

Chichorro, M., Pereira, M. F., Díaz-Azpiroz, M., Williams, I. S., Fernandez, C., Pin, C., & Silva, J. B. (2008). Cambrian ensialic rift-related magmatism in the Ossa-Morena Zone (Évora-Aracena metamorphic belt, SW Iberian Massif): Sm-Nd isotopes and SHRIMP zircão U-Th-Pb geochronology. *Tectonophysics, 461*, 91–113. https://doi.org/10.1016/j.tecto.2008.01.008

Condie, K. C. (1993). Chemical composition and evolution of the upper continental crust: Contrasting results from surface samples and shales. *Chemical Geology, 104*, 1–37. https://doi.org/10.1016/0009-2541(93)90140-E

Cortial, F., Gauthier-Lafaye, F., Lacrampe-Couloume, G., OBerlin, A., & Weber, F. (1990). Characterization of organic matter associated with uranium deposits in the Francevillian Formation of Gabon (Lower Proterozoic). *Organic Geochemistry, 15*(1), 73–85. https://doi.org/10.1016/0146-6380(90)90185-3

Dias, R., Ribeiro, A., Romão, J., Coke, C., & Moreira, N. (2016). A review of the Arcuate Structures in the Iberian Variscides; Constraints and Genetic Models. *Tectonophysics, 681C*, 170–194. https://doi.org/10.1016/j.tecto.2016.04.011

Dill, H. (1986). Metallogenesis of early Palaeozoic graptolite shales from the Graefenthal Horst (northern Bavaria-Federal Republic of Germany). *Economic Geology, 81*, 889–903. https://doi.org/10.2113/gsecongeo.81.4.889

Dypvik, H. (1984). Geochemical compositions and depositional conditions of Upper Jurassic and Lower Cretaceous Yorkshire clays, England. *Geological Magazine, 121*, 489–504. https://doi.org/10.1017/S0016756800030028

Eguíluz, L., Gil Ibarguchi, J. I., Abalos, B., & Apraiz, A. (2000). Superposed Hercynian and Cadomian orogenic cycles in the Ossa-Morena zone and related areas of the Iberian Massif. *Geological Society of America Bulletin, 112*, 1398–1413. https://doi.org/10.1130/0016-7606(2000)112%3c1398:SHACOC%3e2.0.CO;2

El-Anwar, E. A. A., Mekky, H. S., & Wahab, W. A. (2018). Geochemistry, mineralogy and depositional environment of black shales of the Duwi Formation, Qusseir area, Red Sea coast, Egypt.

Carbonates and Evaporites, 34, 883–892. https://doi.org/10.1007/s13146-017-0417-7

Elderfield, H., & Greaves, M. J. (1982). The rare earth elements in seawater. *Nature, 296*, 214–219. https://doi.org/10.1038/296214a0

Emerson, S. R., & Huested, S. S. (1991). Ocean anoxia and the concentrations of molybdenum and vanadium in seawater. *Marine Chemistry, 34*, 177–196. https://doi.org/10.1016/0304-4203(91)90002-E

Fang, X., Wu, L., Geng, A., & Deng, Q. (2019). Formation and evolution of the Ediacaran to Lower Cambrian black shales in the Yangtze Platform, South China. *Palaeogeography, Palaeoclimatology, Palaeoecology, 527*, 87–102. https://doi.org/10.1016/j.palaeo.2019.04.025

Fernández-Suárez, J., Gutiérrez-Alonso, G., & Jeffries, T. E. (2002). The importance of along margin terrane transport in northern Gondwana: Insights from detrital zircon parentage in Neoproterozoic rocks from Iberia and Brittany. *Earth and Planetary Science Letters, 204*, 75–88. https://doi.org/10.1016/S0012-821X(02)00963-9

Ferreira, E., Mateus, A., Azevedo, A. C., Duarte, L. V., Mendonça-Filho, J., & Tassinari, C. C. G. (2020). Tracing bottom-water redox conditions during deposition of Lower and Upper Jurassic organic-rich sedimentary rocks in the Lusitanian Basin (Portugal): Insights from inorganic geochemistry. *Marine and Petroleum Geology, 117*, 104343. https://doi.org/10.1016/j.marpetgeo.2020.104343

Finkelman, R. B., Palmer, C. A., & Wang, P. (2018). Quantification of the modes of occurrence of 42 elements in coal. *International Journal of Coal Geology, 185*, 138–160. https://doi.org/10.1016/j.coal.2017.09.005

Floyd, P. A., & Leveridge, B. E. (1987). Tectonic environment of the Devonian Gramscatho basin, south Cornwall: Framework mode and geochemical evidence from turbiditic sandstones. *Journal of the Geological Society of London, 144*(4), 531–542. https://doi.org/10.1144/gsjgs.144.4.0531

Gao, P., Liu, G., Jia, C., Young, A., Wang, Z., Wang, T., Zhang, P., & Wang, D. (2016). Redox variations and organic matter accumulation on the Yangtze carbonate platform during Late Ediacaran-Early Cambrian: Constraints from petrology and geochemistry. *Palaeogeography, Palaeoclimatology, Palaeoecology, 450*, 91–110. https://doi.org/10.1016/j.palaeo.2016.02.058

Gonçalves, F., & Carvalhosa, A. (1994). O Proterozóico da Zona de Ossa-Morena no Alentejo. Síntese e Atualização de Conhecimentos. *Memórias de Ciências*, 141–173.

Gonçalves, F., & Oliveira, V. (1986). Alguns aspetos do Precâmbrico da Zona de Ossa Morena em Portugal. O Proterozoico Superior de Estremoz. *Memórias Da Academia Ciências De Lisboa, 27*, 111–117.

Gromet, L. P., Dymek, R. F., Haskin, L. A., & Korotev, R. L. (1984). The "North American shale composite": Its compilation, major and trace element characteristics. *Geochemica Et Cosmochimica Acta, 48*, 2469–2482. https://doi.org/10.1016/0016-7037(84)90298-9

Hallberg, R. O. (1976). A geochemical method for investigation of palaeoredox conditions in sediments. *Ambio Special Report, 4*, 139–147.

Hallberg, R. O. (1982). Diagenetic and environmental effects on heavy-metal distribution in sediments: A hypothesis with an illustration from the Baltic Sea. In K. A. Fanning, & F. T. Manheim (Eds), (pp. 305–316). The Dynamic Environment of the Ocean Floor.

Huyck, H. L. O. (1989). When is a metalliferous black shale not a black shale? In *Metalliferous Black Shales and Related Ore Deposits – Proceedings, United States Working Group Meeting* (vol. 1058, pp. 42–56). International Geological Correlation Program Project 254. U. S. Geological Surgery Circular.

Jones, B., & Manning, D. A. C. (1994). Comparison of geochemical indices used for the interpretation of palaeoredox conditions in ancient mudstones. *Chemical Geology, 111*, 111–129. https://doi.org/10.1016/0009-2541(94)90085-X

Ketris, M. P., & Yudovich, Y. E. (2009). Estimations of Clarkes for Carbonaceous biolithes: World averages for trace element contents in black shales and coals. *International Journal of Coal Geology, 78*, 135–148. https://doi.org/10.1016/j.coal.2009.01.002

Kontinen, A., & Hanski, E. (2015). The Talvivaara Black Shale-Hosted Ni-Zn-Cu-Co Deposit in Eastern Finland. In *Mineral Deposits of Finland* (pp. 557–612). Elsevier. https://doi.org/10.1016/B978-0-12-410438-9.00022-4.

Kunzmann, M., Halverson, G. P., Scott, C., Minarik, W. G., & Wing, B. A. (2015). Geochemistry of Neoproterozoic black shales from Svalbard: Implications for oceanic redox conditions spanning Cryogenian glaciations. *Chemical Geology, 417*, 383–393. https://doi.org/10.1016/j.chemgeo.2015.10.022

Laranjeira, V., Ribeiro, J., Moreira, N., Nogueira, P., Mendonça Filho, J., & Flores, D. (2023). Petrographic and geochemical characterization of organic matter of Precambrian black shales from Ossa-Morena Zone, South of Portugal. Springer ASTI. (Accepted).

Large, R. R., Bull, S. W., & Maslennikov, V. V. (2011). A carbonaceous sedimentary source-rock model for carlin-type and orogenic gold deposits. *Society of Economic Geologists, Economic Geology, 106*, 331–358.

Leventhal, J. (1993). *Metals in black shales* (pp. 581–592). Plenum Press.

Leybourne, M. I., Goodfellow, W. D., Boyle, D. R., & Hall, G. M. (2000). Rapid development of negative Ce anomalies in surface waters and contrasting REE patterns in groundwaters associated with Zn–Pb massive sulphide deposits. *Applied Geochemistry, 15*(6), 695–723. https://doi.org/10.1016/S0883-2927(99)00096-7

Liñán, E., & Quesada, C. (1990). Ossa-Morena Zone: Stratigraphy, rift phase (Cambrian). In E. Martinez & R. D. Dallmeyer (Eds.), *Pre-mesozoic geology of Iberia* (pp. 259–266). Springer Verlag.

Linnemann, U., Pereira, M. F., Jeffries, T., Drost, K., & Gerdes, A. (2008). Cadomian Orogeny and the opening of the Rheic Ocean: New insights in the diacrony of geotec-tonic processes constrained by LA-ICP-MS U-Pb zircon dating (Ossa-Morena and Saxo-Thuringian Zones, Iberian and Bohemian Massifs). *Tectonophysics, 361*, 21–43. https://doi.org/10.1016/j.tecto.2008.05.002

LNEG. (2010). *Geological map of Portugal at 1:1 000 000* (3rd ed.). Laboratório Nacional de Energia e Geologia.

Locutura, J., Tornos, F., Florido, P., & Baeza, L. (1990). Ossa-Morena Zone: Metallogeny. In E. Martinez & R. D. Dallmeyer (Eds.), *Pre-mesozoic geology of Iberia* (pp. 321–332). Springer Verlag.

Lopes, L. (2015). *Litogeoquímica na área de concessão da Boa-Fé (Colt Resources)* (132 p.). MSc Thesis (unpublished), Universidade de Aveiro.

Lopes, L., Santos, J. F., Sousa, J. C., & Ribeiro, S. (2015). Novos dados petrográficos, geoquímicos e isotópicos sobre a área de concessão de Boa Fé (Montemor-o-Novo, Zona de Ossa-Morena). In *Comunicações Geológicas* (vol. 102, vol. Especial I, pp. 153–156).

López-Guijarro, R. (2006). Ambiente geodinámico y procedencia de las rocas sedimentarias precámbricas de las zonas de Ossa Morena y Centroibérica a través del análisis geoquímico. *Boletín Geológico Minero, 117*, 499–505.

López-Guijarro, R., Armendáriz, M., Quesada, C., Fernández-Suárez, J., Murphy, J. B., Pin, C., & Bellido, F. (2008). Ediacaran-Palaeozoic tectonic evolution of the Ossa Morena and Central Iberian zones (SW Iberia) as revealed by Sm-Nd isotope systematics. *Tectonophysics, 461*, 202–214. https://doi.org/10.1016/j.tecto.2008.06.006

Maia, M., Moreira, N., Vicente, S., Mirão, J., Noronha, F., & Nogueira, P. (2020). Multi-stage fluid system responsible for ore deposition in the Ossa-Morena Zone (Portugal): Constraints in Cu-ore

deposits formation. *Geology of Ore Deposits, 62*(6), 508–534. https://doi.org/10.1134/S1075701520060094

Maia, M., Roseiro, J., Nogueira, P., Noronha, F., Fuertes-Fuente, M., Cepedal, A., & Mirão, J. (2022). New insights on the Escoural Orogenic gold district (Ossa-Morena Zone, SW Iberia): Geochemistry, fluid inclusions and stable isotope constraints from the Monfurado gold prospect. *Ore Geology Reviews*. https://doi.org/10.1016/j.oregeorev.2022.104736

Mateus, A., Munha, J., Inverno, C., Matos, J.X., Martins, L., Oliveira, D., Jesus, A., & Salgueiro, R. (2013) Mineralizações no sector português da Zona de Ossa-Morena, Geologia de Portugal. In R. Dias, A. Araújo, P. Terrinha, & J.C. Kullberg (Eds) (vol. 1, pp. 577–619) Escolar Editora.

Matos, J. X., & Filipe, A. (2013). Carta de Ocorrências Mineiras do Alentejo e Algarve, Escala 1:400 000 (1st edn). Laboratório Nacional de Energia e Geologia.

Moreira, N., Araújo, A., Pedro, J. C., & Dias, R. (2014a). Evolução geodinâmica da Zona de Ossa-Morena no contexto do SW Ibérico durante o Ciclo Varisco. In *Comunicações Geológicas* (vol. 101, vol. Especial I, pp. 275–278).

Moreira, N., Dias, R., Pedro, J. C., & Araújo, A. (2014b). Interference between Variscan deformation events in Torre de Cabedal structure: Alter-do-Chão – Elvas sector (Ossa-Morena Zone). In *Comunicações Geológicas* (vol. 101, volume Especial I, pp. 279–282).

Moreira, N., Pedro, J., Santos, J. F., Araújo, A., Dias, R., Ribeiro, S., Romão, J., & Mirão, J. (2019). $^{87}Sr/^{86}Sr$ applied to age discrimination of the Palaeozoic carbonates of the Ossa-Morena Zo-ne (SW Iberia Variscides). *International Journal of Earth Sciences, 108*(3), 963–987.

Murray, R. W., Buchholz ten Brink, M. R., Jones, D. L., Gerlach, D. C., & Russ, G. P. (1990). Rare earth elements as indicators of different marine depositional environments in chert and shale. *Geology, 18*, 268–271.

Oliveira, D. P. S., Reed, R. M., Milliken, K. L., Robb, L. J., Inverno, C. M. C., & D'Orey, F. L. C. (2003). Série Negra black quartzites – Tomar Cordoba Shear Zone, E Portugal: Mineralogy and cathodoluminescence studies. *Cuadernos Laboratorio Xeolóxico De Laxe, 28*, 193–211.

Oliveira, D. P. S., Robb, L. J., Inverno, C. M. C., & Charlesworth, E. G. (2007). Metallogenesis of the São Martinho and Mosteiros Gold Deposits, Tomar Cordoba Shear Zone, Portugal. *International Geology Review, 49*(10), 907–930. https://doi.org/10.2747/0020-6814.49.10.907

Oliveira, J. T., Oliveira, V., & Piçarra, J. M. (1991). Traços gerais da evolução tectono-estratigráfica da Zona de Ossa Morena em Portugal. *Cuadernos Laboratorio Xeolóxico De Laxe, 16*, 221–250.

Oliveira, V. (1986). Prospecção de Minérios Metálicos a Sul do Tejo 1. *Geociências, Capítulos, 1–2*, 15–22.

Pereira, M. F., Apraiz, A., Chichorro, M., Silva, J. B., & Armstrong, R. A. (2010). Exhumation of high-pressure rocks in northern Gondwana during the Early Carboniferours (Coimbra–Cordoba shear zone. SW Iberian Massif): Tectonothermal analysis and U-Th–Pb SHRIMP in-situ zircon geochronology. *Gondwana Research, 17*, 440–460. https://doi.org/10.1016/j.gr.2009.10.001

Pereira, M. F., Chichorro, M., Linnemann, U., Eguíluz, L., & Silva, J. B. (2006). Inherited arc signature in Ediacaran and Early Cambrian basins of the Ossa-Morena Zone (Iberian Massif. Portugal): Paleogeographic link with European and North African Cadomian correlatives. *Precambrian Research, 144*, 297–315. https://doi.org/10.1016/j.precamres.2005.11.011

Pereira, M. F., Silva, J. B., Chichorro, M., Ordóñez-Casado, B., Lee, J. K. W., & Williams, I. S. (2012a). Early Carboniferous wrenching, exhumation of high-grade metamorphic rocks and basin instability in SW Iberia: Constraints derived from structural geology and U-Pb and ^{40}Ar-^{39}Ar geochronology. *Tectonophysics, 558–559*, 28–44.

Pereira, M. F., Solá, A. R., Chichorro, M., Lopes, L., Gerdes, A., & Silva, J. B. (2012b). North-Gondwana assembly, break up and paleogeography: U-Pb isotope evidence from detrital and igneous zircons of Ediacaran and Cambrian rocks of SW Iberia. *Gondwana Research, 22*(3–4), 866–881. https://doi.org/10.1016/j.gr.2012.02.010

Pfefferkorn, H. W. (1968). Geologie des Gebietes zwischen Serpa und Mértola (Baixo Alentejo, Portugal). *Munstersche Forschungen Zur Geologieund Palaontologie, 9*, 1–143.

Pi, D. H., Liu, C. Q., Shields-Zhoud, G. A., & Jiang, S. Y. (2013). Trace and rare earth element geochemistry of black shale and kerogen in the early Cambrian Niutitang Formation in Guizhou province. South China: Constraints for redox environments and origin of metal enrichments. *Precambrian Research, 225*, 218–229. https://doi.org/10.1016/j.precamres.2011.07.004

Piercey, S. J., Gibson, H. L., Tardif, N., & Kamber, B. S. (2016). Ambient Redox and Hydrothermal Environment of the Wolverine Volcanogenic Massive Sulfide Deposit, Yukon: Insights from Lithofacies and Lithogeochemistry of Mississippian Host Shales. *Economic Geology, 111*, 1439–1463. https://doi.org/10.2113/econgeo.111.6.1439

Pipper, D. Z. (1974). Rare earth elements in the sedimentary cycle: A summary. *Chemical Geology, 14*, 285–304. https://doi.org/10.1016/0009-2541(74)90066-7

Potter, P. E., Maynard, J. B., & Pryor, W. A. (1980). Sedimentology of shale. In *Study guide and reference source* (310 p.). Springer Verlag. https://doi.org/10.1007/978-1-4612-9981-3.

Quesada, C. (1990). Precambrian terranes in the Iberian Variscan foldbelt. In R. A. Strachan & G. K. Taylor (Eds.), *Avalonian and Cadomian Geology of the North Atlantic* (pp. 109–133). Blackie and Sons.

Quesada, C., & Oliveira, J. T. (2019). The geology of Iberia: A geodynamic approach, Volume 2: The Variscan Cycle (544 p.). Springer International Publishing.

Ribeiro, A., Munhá, J., Dias, R., Mateus, A., Pereira, E., Ribeiro, M. L., Fonseca, P., Araújo, A., Oliveira, T., Romão, J., Chaminé, H., Coke, C., & Pedro, J. (2007). Geodynamic evolution of SW Europe Variscides. *Tectonics, 26*, 2.

Ribeiro, A., Munhá, J., Mateus, A., Fonseca, P., Pereira, E., Noronha, F., Romão, J., Rodrigues, J. F., Castro, P., Meireles, C., & Ferreira, N. (2009). Mechanics of thick-skinned Variscan overprinting of Cadomian basement (Iberian Variscides). *Comptes Rendus Geoscience, 341*(2–3), 127–139.

Ribeiro, J., Machado, G., Moreira, N., Suárez-Ruiz, I., & Flores, D. (2019). Petrographic and geochemical characterization of coal from Santa Susana Basin, Portugal. *International Journal of Coal Geology, 203*(2), 36–51. https://doi.org/10.1016/j.coal.2019.01.005

Ross, D. J. K., & Bustin, R. M. (2009). Investigating the use of sedimentary geochemical proxies for paleoenvironmental interpretation of thermally mature organic-rich strata: Examples from the Devonian-Mississippian shales, Western Canadian Sedimentary Basin. *Chemical Geology, 260*, 17–19. https://doi.org/10.1016/j.chemgeo.2008.10.027

Rudnick, R. L., & Gao, S. (2014). Composition of the continental crust. In *Treatise on Geochemistry* (2nd edn, vol. 3, pp. 1–64) Elsevier. https://doi.org/10.1016/B0-08-043751-6/03016-4.

Sáez, R., Moreno, C., & González, F. (2011). Black shales and massive sulfide deposits: Causal or casual relationships? Insights from Rammelsberg, Tharsis, and Draa Sfar. *Mineralium Deposita, 46*, 585–614. https://doi.org/10.1007/s00126-010-0311-x

Sánchez-Lorda, M. E., Sarrionandia, F., Ábalos, B., Carrracedo, M., Eguíluz, L., & Gil Ibarguchi, J. I. (2014). Geochemistry and paleotectonic setting of Ediacaran metabasites from the Ossa-Morena Zone (SW Iberia). *International Journal of Earth Sciences, 103*, 1263–1286. https://doi.org/10.1007/s00531-013-0937-x

Schäfer, H. J., Gebauer, D., Nagler, T. F., & Eguíluz, L. (1993). Conventional and ion-microprobe U-Pb dating of detrital zircãos of the Tentudía Group (Série Negra, SW Spain): Implications for zircon systematics, stratigraphy, tectonics and the Precambrian/Cambrian boundary. *Contributions to Mineralogy and Petrology, 113*(3), 289–299.

Schieber, J., 1978. Black shales. *In:* Sedimentology. Encyclopedia of Earth Science. Springer, Berlin, Heidelberg.

Shaw, T. J., Geiskes, J. M., & Jahnke, R. A. (1990). Early diagenesis in differing depositional environments: The response of transition metals in pore water. *Geochimica Et Cosmochimica Acta, 54*, 1233–1246. https://doi.org/10.1016/0016-7037(90)90149-F

Sozinov, N. A. (1982). Ore potential of Precambrian black shale formation. *Revista Brasileira De Geociências, 12*(1–3), 506–509.

Suárez-Ruiz, I., Flores, D., Mendonça Filho, J. G., & Hackley, P. C. (2012). Review and update of the applications of organic petrology: Part 1, geological applications. *International Journal of Coal Geology, 99*, 54–112. https://doi.org/10.1016/j.coal.2012.02.004

Taylor, S. R., & McLennan, S. M. (1985). *The continental crust: Its composition and evolution*. Blackwell Scientific Publications.

Tornos, F., Casquet, C., Relvas, J., Barriga, F., & Sáez, R. (2002). Transpressional tectonics and ore deposit formation: the southwestern margin of the Iberian Variscan Belt. In D. Blundell, F. Neubauer, & A. Von Quadt (Eds.), *The timing and location of major ore deposits in an evolving orogeny* (Vol. 206, pp. 179–198). Geological Society of London, Special Publications.

Tornos, F., Inverno, C. M. C., Casquet, C., Mateus, A., Ortiz, G., & Oliveira, O. (2004). The metallogenic evolution of the Ossa-Morena Zone. *Journal of Iberian Geology, 30*, 143–181.

Tourtelot, B. (1979). Black shale: Its deposition and diagenesis. *Clays and Clay Minerology, 27*, 313–321. https://doi.org/10.1346/CCMN.1979.0270501

Trabucho-Alexandre, J. (2014). More gaps than shale: Erosion of mud and its effect on preserved geochemical and palaeobiological signals. *Geological Society of London, Special Publication, 404*(1), 251. https://doi.org/10.1144/SP404.10

Tribovillard, N., Algeo, T. J., Lyons, T., & Riboulleau, A. (2006). Trace metals as paleoredox and paleoproductivity proxies: An update. *Chemical Geology, 232*, 12–32. https://doi.org/10.1016/j.chemgeo.2006.02.012

Vegas, K. (1968). Sobre la existencia de Precambrico en la Baja Extremadura. *Estudios Geológcos, 24*, 85–89.

Wang, N., Li, M., Hong, H., Song, D., Tian, X., Liu, P., Fang, R., Chen, G., & Wang, M. (2019). Biological sources of sedimentary organic matter in Neoproterozoic-Lower Cambrian shales in the Sichuan Basin (SW China): Evidence from biomarkers and microfossils. *Palaeogeography, Palaeoclimatology, Palaeoecology, 516*, 342–353. https://doi.org/10.1016/j.palaeo.2018.12.012

Wedepohl, K. H. (1971). Environmental influences on the chemical composition of shales and clays. *Physics and Chemistry of the Earth, 8*, 305–333. https://doi.org/10.1016/0079-1946(71)90020-6

Wignall, P. B. (1994). *Black shales* (p. 127). Clarendon Press.

Wilde, P., Quinby-Hunt, M. S., & Erdtmann, B. (1996). The whole-rock cerium anomaly: A potential indicator of eustatic sea-level changes in shales of the anoxic facies. *Sedimentary Geology, 101*(1–2), 43–53. https://doi.org/10.1016/0037-0738(95)00020-8

Affiliations

V. Laranjeira[1,2] · J. Ribeiro[3,4] · N. Moreira[5,6,7] · P. Nogueira[8,9] · D. Flores[1,2]

J. Ribeiro
joana.ribeiro@uc.pt

N. Moreira
nafm@uevora.pt

P. Nogueira
pmn@uevora.pt

D. Flores
dflores@fc.up.pt

[1] Present Address: Department of Geosciences, Environment and Spatial Planning, University of Porto, Rua Do Campo Alegre, 4169-007 Porto, Portugal

[2] Institute of Earth Sciences, Pole of University of Porto, Rua Do Campo Alegre, 4169-007 Porto, Portugal

[3] Department of Earth Sciences, University of Coimbra, Rua Sílvio Lima, 3030-790 Coimbra, Portugal

[4] Institute of Earth Sciences, Pole of University of Porto, Rua Do Campo Alegre, 4169-007 Porto, Portugal

[5] Institute of Earth Sciences, Colégio Luís António Verney, Pole of University of Évora, Rua Romão Ramalho, 59, 7000-671 Évora, Portugal

[6] Department of Geosciences, Colégio Luís António Verney, University of Évora, Rua Romão Ramalho, 59, 7000-671 Évora, Portugal

[7] Instituto de Investigação e Formação Avançada (IIFA), Colégio Luís António Verney, University of Évora, Rua Romão Ramalho, 59, 7000-671 Évora, Portugal

[8] Department of Geosciences, Colégio Luís António Verney, University of Évora, Rua Romão Ramalho, 59, 7000-671 Évora, Portugal

[9] Institute of Earth Sciences, Colégio Luís António Verney, Pole of University of Évora, Rua Romão Ramalho, 59, 7000-671 Évora, Portugal